PUB-77-118-E
E-0031

E31A

ANL-HEP-PR-77-39

Properties of the Hadronic System Resulting from $\bar{\nu}_\mu$ p Interactions*

M. DERRICK, P. GREGORY, L. G. HYMAN, K. JAEGER, D. LISSAUER+, R. J. MILLER, B. MUSGRAVE, J. J. PHELAN, P. SCHREINER, and R. SINGER

Argonne National Laboratory, Argonne, Illinois 60439

and

S. J. BARISH, A. ENGLER, G. KEYES, T. KIKUCHI, and R. KRAEMER

Carnegie-Mellon University, Pittsburgh, Pennsylvania 15213

and

V. E. BARNES, D. D. CARMONY, A. F. GARFINKEL, and A. T. LAASANEN

Purdue University, West Lafayette, Indiana 47907

The properties of the final state hadronic system in anti-neutrino-proton charged-current interactions are presented. The events were observed in the Fermilab 15-foot hydrogen bubble chamber. The average energy of the events is ~ 30 GeV, but there are some interactions beyond 100 GeV. The mean multiplicity of the charged hadrons varies as $< n_C^H > = (0.06 \pm 0.06) + (1.22 \pm 0.03)\, \ell n\, W^2$ for hadronic masses W in the range $1.0 < W^2 < 50\ \mathrm{GeV}^2$. By contrast, the multiplicity depends only weakly on the four-momentum transfer between the leptons. The mean pion multiplicities for events with 3- or more charged tracks are found to be $< n_- > = 1.64 \pm 0.04$, $< n_0 > = 1.16 \pm 0.13$, for π^- and

*Work supported by the U. S. Energy Research and Development Administration.

+Present Address: Tel-Aviv University, Tel-Aviv, Israel.

π^0 production, respectively. By comparing the number of positive tracks with π^- data from neutrino production, we deduce a mean proton multiplicity $< n_p >$ of 0.53 ± 0.15. The single-particle distributions in both longitudinal and transverse momentum are found to be similar to those for non-diffractive production in hadronic collisions. The fragmentation properties of the final state d quarks are compared to the expectations of the quark parton model. The fraction of observed neutral strange-particle production for events with 3- or more charged tracks is 0.08 ± 0.015 and is consistent with coming completely from associated production.

I. Introduction

In this paper, we discuss the properties of the neutral hadronic system H^0 formed in charged-current (CC) antineutrino proton interactions:

$$\bar{\nu} p \rightarrow \mu^+ H^0 \quad .$$

The gross features of multiparticle production in both hadronic and virtual photon-induced reactions are known to depend principally on the available center-of-mass energy and only weakly on the specific quantum numbers of the projectile and target. There are, however, very few data available using neutrino beams, particularly on a simple target such as hydrogen. Although our data are of limited statistical accuracy, they clearly exhibit that the dominant features of the hadronic system from $\bar{\nu}p$ CC reactions are similar to those observed using other incident particles.

The data on inclusive scaling variable distributions in ν and $\bar{\nu}N$ collisions on the other hand show regularities that are simply explained by the ideas of the quark-parton-model (QPM). It is of great interest to extend these

tests to the detailed properties of the hadronic system, and there has been considerable recent interest in such studies for both leptonic reactions and hadronic collisions at high $p_\perp$. The quarks emerging from the violent collisions are thought to fragment into hadrons in a characteristic way that reveals the quantum numbers of the quark produced in the primary current-quark or quark-quark interaction. Although only a fraction of our data is in the kinematic regime where these ideas should apply, our experiment supports the general validity of the ideas of the QPM. Specifically, our results show the universal quark fragmentation function expected on this model.

II. Experimental Details

The data sample was obtained from two separate exposures of the Fermilab 15-foot hydrogen bubble chamber to a broad-band antineutrino beam. The beam was produced for the two exposures by focussing negative particles coming from an Al target bombarded by incident proton beams of 300 and 400 GeV, respectively. The 300 GeV run, with a single magnetic horn, yielded 24,000 pictures. The 400 GeV run, using two horns, yielded 38,000 pictures. The neutrino background flux was at the 10% level except for the highest $\bar{\nu}$ energies.[1, 2]

In the scan of the film, events of all topologies except one-prongs were recorded provided the total momentum in the forward hemisphere exceeded 2 GeV/c. The overall scanning efficiency was (98 ± 2)%. Track reconstruction was made using a modified version of the program TVGP. After repeated measurements, 87% of the events were successfully reconstructed. The losses are multiplicity-dependent and have been corrected in the data presented. The raw event sample consists of (1) the $\bar{\nu}p$ charged current (CC)

events that are the subject of the present paper, (2) νp CC events, (3) $\bar{\nu}p$ and νp neutral current (NC) events, and (4) neutron-induced events:

$$\bar{\nu}p \rightarrow \mu^+ H^o \quad (1)$$

$$\nu p \rightarrow \mu^- H^{++} \quad (2)$$

$$\bar{\nu}p \rightarrow \bar{\nu}\, H^+ \quad (3a)$$

$$\nu p \rightarrow \nu\, H^+ \quad (3b)$$

$$np \rightarrow \text{anything} \quad . \quad (4)$$

The background from K_L^o mesons was found to be negligible. The incident neutron spectrum was determined by kinematically fitting all three-prong events to the 1-constraint hypothesis

$$np \rightarrow pp\pi^- \quad . \quad (5)$$

No evidence for reaction (5) was observed for events with visible vector momentum (P_{vis}) greater than 5 GeV/c.[2] Based upon this fact and the calculated shape of the incident antineutrino flux, we required that the candidates for the charged-current reactions have a $P_{vis} \geq 5$ GeV/c. With this selection, we expect no neutron-induced events in the selected $\bar{\nu}p$ data.

Empirical muon selection criteria for the separation of the CC and NC events have been developed in a Monte Carlo simulation of events produced by the incident antineutrino and neutrino fluxes.[3] The highest momentum track was taken as the muon candidate if the ratio of its momentum to that of the second highest was greater than 2. When this ratio was less than 2, the track with the highest transverse momentum exceeding 1 GeV/c was chosen as the muon candidate. If the hadronic tracks had a total transverse momentum opposite to that of the muon candidate, the event was accepted as a CC

event. When the muon and the hadronic system lay on the same side of the beam and the cosine of the vector sum of the hadronic momentum was $>(<)\ 0.9$ relative to the beam direction, the event was classified as a CC (NC) event. The Monte Carlo program indicated that for events with $\geq$ 3-prongs, this prescription selected $\sim$ 90% of the true $\bar{\nu}$ CC events, with a contamination from reactions (2) and (3) of $\sim$ 12%. Although in most cases we have corrected the distributions given in this paper for the small biases introduced by our selection criteria, the uncertainties arising from the corrections are always less than the statistical errors. The final selected data sample consists of 432 $\bar{\nu}$p CC events.

The pictures were taken in conjunction with the external muon identifier (EMI) placed behind the 15-foot bubble chamber.[4] Where appropriate, this additional data have been used to provide an independent estimate of background contamination. Good agreement is found with the results of our Monte Carlo simulation.

The measurement of the beam energy for events with missing neutrals was made using a modification of a method due to Grant[5] in which the energy is parameterized in terms of the transverse momentum of the missing neutral system relative to the total hadron direction. The antineutrino energy resolution, as calculated from the Monte Carlo simulation, is $\pm 8\%$.[3] Some of the kinematic variables used in this paper are summarized in Fig. 1.

The 1-prong events are difficult to find on this film. In addition, since they consist of a single μ^+ track, no information is available on the kinematic

quantities of the hadronic system. For these reasons, the 1-prong events are not included in the present data sample. Results are usually only given for events with $\geq$ 3-prongs. However, in the cases where we believe this omission may distort the physics, we have included a 1-prong sample generated from the Monte Carlo simulation. We assign an arbitrary 20% systematic error to these events. Distributions with this Monte Carlo simulation included are specifically labelled as such.

The distributions in the total hadronic mass, W, and in the four-momentum transfer squared, Q^2, for events with $\geq$ 3-prongs are shown in Fig. 2. The W distribution is seen to be dominated by a broad maximum in the low-mass region, $2 < W < 5$ GeV. The Q^2 distribution falls monotonically and has a median of 5.2 $(GeV/c)^2$, but it extends beyond 26 $(GeV/c)^2$. In presenting the gross properties of the hadronic system and comparing our results with data obtained from reactions induced by other projectiles, we do not make any selections on W or Q^2. We note that about two-thirds of our data have $W > 2$ GeV and $Q^2 > 1$ $(GeV/c)^2$, which has traditionally been considered the scaling region for studies of the inclusive distributions at the lepton vertex, although there is evidence that the inclusive distributions scale for lower values of W and Q^2.[6]

III. Multiplicity Distributions

a. Charged Multiplicities

In principle, the multiplicity may be a function of Q^2, E_{ν}, and W. The Q^2 dependence of the charged multiplicity is shown in Fig. 3. While the average hadronic prong number shows a rise at low Q^2, it is otherwise Q^2

independent as previously observed in νp data[7] and electroproduction data.[8, 9]

The charged hadronic multiplicity distribution is given in Table I as a function of W and in Table II as a function of E_{ν} for three W intervals. Fig. 4 shows the charged multiplicity distribution for these three W ranges. Both the average multiplicity and the width of the distributions increase with increasing W. The widths, however, are narrower than for a Poisson distribution, as we shall discuss below.

As seen in Table II, the average multiplicity for fixed W is also substantially independent of E_{ν}; thus, the only strong dependence is on W, and a fit to the data over the range $1.0 < W^2 < 50$ GeV^2 yields

$$< n_C^H > = (0.06 \pm 0.06) + (1.22 \pm 0.03) \ln W^2 \quad .$$

Our results for the mean charged hadronic multiplicity, $< n_C^H >$, as a function of W^2 are compared in Fig. 5 to that for neutrino,[7] photoproduction[10] and electroproduction[8] data. It is apparent that the behavior of $< n_C^H >$ is similar in all these processes though the neutrino data lie about half a unit higher than the other reactions, presumably because of charge conservation effects and the low overall multiplicities.

The universality of the W dependence of $< n_C^H >$, shown in Fig. 5, may be extended to annihilation processes, both hadronic ($\bar{p}p$, $\bar{K}K$) and electromagnetic ($\bar{e}e$).[11] Fig. 6 compares our data for the mean number of negative particles $< n_- >$ with that from annihilation data. While for low W^2 the antineutrino data lie below the trend of the annihilation, for $W^2 \gtrsim 5$ GeV^2, the behavior is quite similar though the antineutrino data remains

slightly lower. The deviation at low W^2 is probably related to the presence of a baryon in the $\bar{\nu}p$ final state. Note the strong contrast of the annihilation and $\bar{\nu}p$ results to pp data, where important leading particle effects are present.

The final column of Table I gives the value of the integrated correlation function f_2^{--} defined as

$$f_2^{--} = \langle n_-(n_- - 1)\rangle - \langle n_-\rangle^2 \quad ,$$

where n_- represents the number of negative hadrons. As is well known, f_2 is a measure of the width of the multiplicity distribution. While the width of the distribution increases with W, the increasingly negative values in Table I indicate that the multiplicity distribution becomes increasingly narrower than a Poisson distribution. Fig. 7 compares f_2^{--} in $\bar{\nu}p$ interactions with $\bar{p}p$ annihilation (both on-shell and off-shell) and pp data.[11] The antineutrino data are again consistent with the trend of the annihilation data though lying higher. The marked contrast observed between the behavior of the $\bar{p}p$ annihilation and the pp results has been conjectured as being due in part to the absence of diffractive processes in the former, and in part to a single cluster picture of the annihilation in contrast to multicluster emission in pp reactions. The similarity of the behavior of the antineutrino data with that from annihilation is consistent with the small contribution of diffraction in the former.

b. π^o Multiplicities

The mean number of neutral pions $\langle n_0 \rangle$ for a given number of negative tracks may be measured from a count of associated γ-rays converting in the

liquid hydrogen. Since the total number of observed γ-rays was only 78, the method of determining the mean conversion probability by weighting each γ-ray individually was not used. Instead, we calculated an average weight for each multiplicity by means of a Monte Carlo program which assumed that the laboratory momentum spectrum of the neutral pions was the same as that of the negative pions.

An independent method of determining $< n_0 >$ comes from an examination of the transverse momentum balance in the $\mu\bar{\nu}$ plane. If we make the plausible assumption that the mean value of the transverse momentum relative to the beam $< p_T >$ carried by the charged and neutral hadrons is proportional to the number of particles in the charged and neutral system, then the average number of neutrals is given by

$$< n^H_{neut} > = \frac{< p_T - p^H_{T_C} >}{< p^H_{T_C} >} \cdot < n^H_C > \quad ,$$

where the notation is self-evident.

After correcting the data for the presence of neutrons and unseen V^o's,[12] assuming the same $< p_T >$ for all particles, the results of the two methods are compared in Fig. 8 and Table III. The agreement is excellent. A fit to the γ-ray data yields

$$< n_0 > = (0.57 \pm 0.19) + (0.37 \pm 0.07)\, n_- \quad .$$

Table III also lists the data for $< n_0 >$ versus n_- as measured in νp interactions.[13] The $< n_0 >$ values for the latter are consistently about two standard deviations higher than measured in our experiment. Recalling from Fig. 5 that the average number of charged tracks as a function of W is also higher for νp reactions than for $\bar{\nu} p$ reactions, this result is somewhat

surprising since we might naively expect that the total mean multiplicity at a given value of W would be the same.

IV. Single Particle Distributions

Before discussing differential distributions, it is useful to establish some definitions. Plots will generally be displayed in the center-of-mass system of the virtual W^- and target proton (Fig. 1b) in which the direction of the W^- defines the positive longitudinal axis. Distributions are usually normalized to the total number of $\bar{\nu}\, p \rightarrow \mu^+ H^o$ events. In order to make this normalization, we assume that the one-prong contribution to the $\bar{\nu}\, p \rightarrow \mu^+ H$ cross section is 15% of the total. This result is based on two independent methods: an extrapolation of the observed Y distribution to Y = 0, and estimates of the quasielastic, single π^o, and multi-π^o production cross sections based on low energy data.[14]

We found that protons are only identifiable by bubble density up to 1.0 GeV/c in momentum. Thus, while all negative tracks may be taken as π^- to first order, a complete separation of π^+ and proton tracks is not possible. The π^+ distributions shown below are selected as all positive tracks with identified protons removed. The data sample contains 646 π^- and 59 identified proton tracks. The resolutions in X_F, Y_R, Z and $p_\perp^2$ (defined below) were determined from the Monte Carlo program to be ± 0.05, ± 0.2, ± 0.05, and ± 0.02 $(GeV/c)^2$, respectively.

a. Longitudinal Distributions

Fig. 9 shows the distributions in the invariant structure functions, defined as:

$$F_1(X_F) = \frac{1}{N_T} \frac{2}{\pi \sqrt{s}} \int_0^\infty E^* \frac{d^2N}{dX_F dp_\perp^2} dp_\perp^2$$

and

$$F_2(Y_R) = \frac{1}{N_T} \frac{1}{\pi} \int_0^\infty \frac{d^2N}{dY_R dp_\perp^2} dp_\perp^2 \quad ,$$

plotted as a function of the Feynman variable X_F and of rapidity Y_R. The distributions of the identified protons are also given. The most obvious feature of these plots is the absence of any strong forward diffractive peaks such as are observed in both hadroproduction and photoproduction. As we discussed in the previous section, the absence of diffraction is consistent with the narrow multiplicity distribution observed in $\bar{\nu}$ p reactions. It is apparent that the target fragmentation region shows a steeper X_F dependence for both π^+ and π^- than does the current (W^-) fragmentation region.

Fig. 10 compares the shape of $F_1(X_F)$ in real and virtual photon reactions $\gamma(\gamma_v)p \to \pi^- X^{(15)}$ with our $\bar{\nu}$ data. For this comparison, the $\bar{\nu}$ data are normalized to the γ_v data. Although the γ_v data are restricted in W and Q^2 while the $\bar{\nu}$ data are uncut, the general similarity of shape is evident. Our W distribution has a mean value of about 3 GeV, and so is similar to the W values of the γ data. Note that in the photon reactions, it is necessary to go to finite Q^2, where diffractive vector-meson production is small, before universality in the current fragmentation region is seen.

A similar result is seen if we compare our $\bar{\nu}$ p data to non-diffractive hadroproduction. Fig. 11 displays the $F_1(X_F)$ distribution for the reaction $\pi^+ p \to \pi^- X^{(16)}$ at 8 GeV/c compared to the $\bar{\nu}$ data. Again, the shapes of the two distribution are remarkably similar.

b. Transverse Distributions

The normalized $p_\perp^2$ distribution $\frac{1}{N_T}\frac{dN}{dp_\perp^2}$ for π^+, π^- and identified proton production is shown in Fig. 12. We define $p_\perp$ to be the transverse momentum with respect to the direction of the hadronic system. Apart from a possible excess of π^- tracks at very low $p_\perp^2$, no significant difference in behavior between π^+ and π^- is apparent. A fit to the data for the range $(0.04 < p_\perp^2 < 1.2)$ $(GeV/c)^2$ gives

$$\frac{1}{N_T}\frac{dN}{dp_\perp^2} = (7.5 \pm 0.7)\, e^{-(5.7 \pm 0.4)\, p_\perp^2} .$$

This slope of (5.7 ± 0.4) GeV/c^{-2} is remarkably similar to the values obtained in two separate muon scattering experiments in liquid hydrogen. The Chicago-Harvard-Illinois-Oxford collaboration,[17] with primary energies of 100 and 150 GeV/c, fitted a slope of 5.9 $(GeV/c)^{-2}$, while the Santa-Cruz-Stanford collaboration,[18] with a 14 GeV beam observed a slope of 5.3 $(GeV/c)^{-2}$. Both experimental groups imposed kinematic selections which are given in the references. The steep component at low $p_\perp^2$ occurs in the central region (small $|X_F|$ and is also observed in the Santa-Cruz-Stanford experiment, and indeed in hadronic experiments.[19]

Fig. 13(a, b) show the dependence of $< p_\perp >$ on the hadronic longitudinal inclusive variables X_F and Y_R. Again, νp data are included for comparison.[20, 21] Although the latter has a W selection of $W > 4$ GeV in Fig. 13(a) and $W > 5$ GeV in Fig. 13(b), the data are again similar (except that the high W selection gives the former a wider plateau in Y_R) and behave in the same way as hadronic data. The seagull effect is seen in X_F, while $< p_\perp >$ is lower away from the central region in Y_R.

V. Comparison with Quark-Parton Model

a. Z. Distributions

The quark-parton model makes several clear predictions for single

hadron production in the current fragmentation region. Because in this region hadrons are just the fragments of a single quark, the properties of the hadronic system should be dependent only on the variable Z and be independent of other variables such as $E_{\bar{\nu}}$, X and Y, or Q^2 and W. The Z distributions of hadrons, $D^h(Z) = \frac{1}{N_T}\frac{dN}{dZ}$, is a measure of the probability distribution for a fragmenting quark to produce a hadron of fractional energy Z. Fig. 14 compares the normalized Z distribution for charged hadrons for three ranges of $E_{\bar{\nu}}$. For $Z \geq 0.3$, scaling does appear to be satisfied.

A more precise test of the QPM can be made by examining the absolute value of the Z distribution for π^- production. If we ignore the contribution of 'sea' quarks, the recoiling quark is a d or u quark in $\bar{\nu}$ p and ν p scattering, respectively, while in γp, it is (8/9) u + (1/9) d. Two independent predictions of $D_d^{\pi^-}(Z)$ have been made by Feynman and Field[22] and by Sehgal.[23] Sehgal's curve is based purely on a fit to electroproduction data while Feynman and Field have also included neutrino data and imposed constraints on the high Z behavior of the D function. The comparison with our $\bar{\nu}$p data is shown in Fig. 15. Again, for $Z \geq 0.3$, the agreement is good in both cases, with the Feynman and Field curve giving slightly better agreement.

While we saw previously that the universality of the X_F distribution appears to extend to hadroproduction, where manifestly the ideas of the quark-parton model are not appropriate, the important point is that there we saw a universality of shape only. In this case not only the shape but the absolute normalization of the Z distribution is successfully predicted. Also shown in Fig. 15 is a prediction of the Z distribution made by Seiden[24] based upon quark-fragmentation functions deduced from particle ratios measured in high-transverse-momentum pp scattering. In this case, the prediction does not agree well with our data.

Fig. 16 shows the ratio of produced positive to negative hadrons for

$Z \geq 0.2$ as a function of X, Y, Q^2 and W. (We stretch the definition of the quark fragmentation region a little because of statistical limitations.) The data are reasonably consistent with a ratio independent of the four variables though the value appears to fall with increasing W and Y, while a dip is also seen at high Q^2. Since there are no obvious W or Q^2 thresholds in these distributions, we cannot use them to set the scale for selecting quark jets. The imposition of the W and Q^2 selections of $W > 2$ GeV and $Q^2 > 1$ $(GeV/c)^2$ makes little difference to these distributions, merely flattening the small Y behavior and slightly reducing the ratio at small X.

b. Mean Transverse Momentum

A second check of the ideas of current-quark scattering and quark fragmentation can be obtained from the dependence of the average $p_\perp$ for positive and negative tracks on the scaling variables X and Z (Fig. 17(a, b)), and on Q^2 and W^2 (Fig. 17(c, d)). Where results are available, we also show the ν p and μp data.[13, 18] The mean $p_\perp$ in the neutrino data is measured with respect to the charged component of the hadronic vector. The difference between $< p_\perp >$ relative to this axis and $< p_\perp >$ relative to the total hadronic vector should, however, be small though the latter will always be larger. The mean transverse momentum, $< p_\perp >$, is seen to be independent of X as the QPM requires, while in terms of Z, it rises quickly for Z below 0.3 and then plateaus. This behavior also indicates that $Z > 0.3$ defines the d quark fragmentation region. The z-independence of $< p_\perp >$ for the quark jet indicates that the longitudinal and transverse dependencies are separable.

Fig. 17(c) shows that $< p_\perp >$ is also substantially independent of Q^2 for both ν p and $\bar{\nu}$ p though a slight rise at low Q^2 is apparent. Similar behavior is observed in electroproduction.[15] The plot of $< p_\perp >$ against W^2 (Fig. 17(d)),

however, is rather puzzling. The neutrino data, though showing a slight rise at low W^2, are essentially flat. Our antineutrino data, however, have a somewhat larger rise at low W^2 and perhaps levels out at a higher $< p_\perp >$ than the neutrino data. The 14 GeV/c Santa Cruz-Stanford $\mu^+ p$ experiment also shows a continuous rise of $< p_\perp >$ with W^2,[18] and shows the steepest slope for high positive X_F ($0.4 \leq X_F < 0.9$), which are the data shown in Fig. 17(d). This X_F region is where the QPM should be most applicable. Clearly, this phenomenon needs further investigation and may be connected with the transverse momentum distribution of the quarks within the proton.

c. Quark Charges

Feynman[25] has suggested that the quantum numbers of a scattered quark would be retained, on the average, in the hadronic jet in the quark fragmentation region. Within the quark-parton model (QPM), the flavor of the scattered quark is well defined in neutrino ($d \rightarrow u$) and antineutrino ($u \rightarrow d$) deep inelastic scattering, and one might hope to observe the charge of this quark and of the recoiling di-quark system in the appropriate rapidity regions of the hadronic system. However, Farrar and Rosner[26] pointed out that Feynman's hypothesis need not be correct, but is modified by the average properties of the quark sea. Brodsky and Weiss[26] have recently discussed quark charge distributions for positive and negative hadrons. In Fig. 18(a) we show $(dN^+/dY_R - dN^-/dY_R)$ for our antineutrino-proton data with the selection $W \geq 3$ GeV. This cut was motivated by the fall of N_H^+/N_H^- seen in Fig. 16 and by the behavior of $< p_\perp >$ of Fig. 17 Since there is no strong Q^2 dependence at low Q^2 for either of these two quantities, we do not make any Q^2 selection for the data of Fig. 18. For comparison, the corresponding neutrino data[20] are displayed in Fig. 18(b). The dotted lines show the observed mean charge for positive and negative Y_R averaged over the regions covered by the lines.

Qualitatively, these low statistics data yield charge distributions as expected from the naive QPM, even though the total hadronic energy is small and the data include the quark sea contribution.

VI. Estimate of the Proton Multiplicity

The scale invariance of the Z distributions in the current fragmentation regions of νp and $\bar{\nu}$ p scattering allows us to estimate the number of final state protons in our experiment. Isospin invariance demands that the fragmentation of a d quark into π^- is identical to the fragmentation of a u quark into π^+. It therefore follows that the Z distribution in the current fragmentation region for $\bar{\nu}p \rightarrow \mu^+\pi^+X$ should be the same as $\nu p \rightarrow \mu^-\pi^-X$. Fig. 19(a) displays the comparison of $1/N_T\ dN/dZ$ for the latter[27] with that for $\bar{\nu}p \rightarrow \mu^+h^+X$, where h^+ represents any positive hadron. The reader should note that the data of Fig. 19 are uncorrected. We assume that the difference between the two data samples for $Z > 0.25$ is due to protons. This difference is plotted in Fig. 19(b) together with the normalized distribution for identified protons.[28] Since for $Z < 0.05$, all protons are identified, the difference curve may be extrapolated to a known point at $Z = 0$. Integrating over the area under the curve of Fig. 19(b) leads to an estimate of 230 ± 60 protons in our sample or 0.53 ± 0.15 protons per event for 3-prongs and above. The average number of π^+ per event for 3-prongs and above then becomes 1.11 ± 0.16 as compared to 1.64 ± 0.04 for π^- and 1.16 ± 0.13 for π^0 production. Thus, the mean number of π^0's $\langle n_0 \rangle$ is consistent with the relation

$$2\langle n_0 \rangle = \langle n_+ \rangle + \langle n_- \rangle \quad .$$

VIII. Strange Particle Production

The study of strange particle production is of special interest since such events can shed light on the characteristics of the quark distributions within the proton. The only valence quark interaction that would give strange particles in the final state is

$$\bar{\nu} u \rightarrow \mu^+ s \quad , \tag{6}$$

whereas from the $q\bar{q}$ sea one can have the reactions

$$\bar{\nu}(c\bar{c}) \rightarrow \mu^+(s\bar{c}) \tag{7}$$

$$\bar{\nu}\ (s\bar{s}) \rightarrow \mu^+(s\bar{c}) \tag{8}$$

and

$$\bar{\nu}(s\bar{s}) \rightarrow \mu^+(s\bar{u}) \quad . \tag{9}$$

Reactions (6) and (9) are suppressed by a $\sin^2\theta_c$ Cabbibo factor, and since reaction (9) also involves the $q\bar{q}$ sea, it should be very small. Reactions (7) and (8) would predominantly give a final state with two strange particles, although such associated production can also result from the fragmentation of a non-strange quark or from the decay of a high mass N^*. The overall rates of reactions (6) to (9) are expected to be a few percent.[29]

Decays of neutral strange particles have been searched for and kinematically fitted to the $\Lambda \rightarrow p\pi^-$, $\bar{\Lambda} \rightarrow \bar{p}\pi^+$, and $K^o_s \rightarrow \pi^+\pi^-$ hypotheses. In the antineutrino charged-current events with 3- or more prongs, we find a total of 32 events with one or more seen associated strange particles corresponding to $(7 \pm 1)\%$ of the CC events. The numbers of events and corrected rates are summarized in Table IV. Our data are consistent with coming completely from associated production.

If we therefore neglect reactions (6) and (9) and if we also assume $K^+K^- = K^+\bar{K}^o = K^-K^o = K^o\bar{K}^o$ and that $\Lambda K^o = \Lambda K^+$, then we find a lower limit for associated production in charged-current antineutrino interactions of 20%. This

is much larger than the rate expected for reactions (7) and (8) above and, therefore, associated production is not dominated by these reactions.

Our event numbers are too small to separate the contribution of single strange particle production in a statistical manner. As an alternative technique, we have made constrained kinematic fits at the production vertex to strangeness-changing hypotheses for all events with visible strange particles. No fits were found corresponding to a 90% confidence upper limit of 0.5% for such reactions. Considering that we cannot recognize charged kaons and that the mean π^o multiplicity is about one, this limit is not inconsistent with the few percent total rate expected for reaction (6).

Fig. 20 compares the rate of visible V^o production as a function of W in γp,[9, 30] μp,[31] νp,[32] and $\bar{\nu} N$[33] reactions. The rates of all these processes are seen to be consistent with each other, with strange particle production increasing with W in the range $2 < W < 10$ GeV.

Fig. 21 compares the uncorrected inclusive distributions of events with strange particles with the equivalent distributions for all charged-current antineutrino events in the E_ν and Q^2 plots. While the strange-particle events fall at higher Y and lower X than the overall data, this is expected from the higher threshold in W for the former.

The distributions of Y_R and $p_\perp^2$ are shown in Fig. 22 for K^o and Λ^o separately. A tendency for the Λ's to be produced in the target fragmentation region is evident, while K^o production resembles pion production. For K^o's

we find $< Y_R > = 0.21 \pm 0.12$ and $< p_\perp^2 > = 0.24 \pm 0.07$ (GeV/c)^2, similar to the means for charged pion production, $< Y_R > = 0.25 \pm 0.03$ and $< p_\perp^2 > = 0.19 \pm 0.01$ (GeV/c)^2.

VII. Exclusive Channels

A systematic attempt was made to fit all events with $\Sigma P_{vis} > 5$ GeV/c to possible charged-current hypotheses with no missing neutral particles using the program SQUAW. In order for a fit to be accepted, the muon track was required to agree with EMI information where available and with the kinematic muon selection criteria.

The accepted fits are listed in Table V. The pion-nucleon effective mass and Q^2 distributions for the single-pion production channel are shown in Fig. 23. The overall distribution in Q^2 shows substantial production for $Q^2 > 2$ GeV^2, which is surprising in view of the form factor damping observed in simple reactions at lower neutrino energies. We estimate that the data sample could contain as much as 30% contamination from channels with associated neutral particles. Based on lower energy measurements,[14] we expect 8.5 $\mu^+\Delta^0$ events. There are 9 events with $m_{p\pi^-} < 1.4$ GeV, but inspection of Fig. 24(a) makes it clear that an estimate of the $\mu^+\Delta^0$ production cannot be made with our present statistics. For the five- and seven-particle final states, our data are too limited in statistics to draw any clear conclusions about the quantity of resonance production in $\bar{\nu}p$ reactions. A search was made for the reaction $\bar{\nu}p \rightarrow \mu^+ p A_1^-$ followed by the decay $A_1^- \rightarrow \pi^+\pi^-\pi^-$. After imposing the selections $Q^2 \leq (10$ GeV/c$)^2$, $|t_{pp}| \leq 2$ (GeV/c)^2, and $0.68 \leq$

$m_{\pi^+\pi^-} \leq 0.84$ GeV in order to enhance diffractive A_1 production, we observe at most 2 events in the A_1 mass region. This corresponds to a cross section ratio of $\sigma(\bar{\nu}p \rightarrow \mu^+ A_1^- p)/\sigma_T = 0.008 \pm 0.006$ averaged over all the flux spectrum. Some recent theoretical predictions[34] are compatible with such a ratio.

IX. Summary

The properties of the hadronic system in $\bar{\nu}p$ charged-current reactions have been examined and compared to νp, electroproduction, and non-diffractive hadroproduction. The gross features of the data appear to be the same in all these processes. Predictions of the QPM in terms of the behavior of charge ratios, Z distributions, and mean $p_\perp$ are generally substantiated. Strange-particle events are found to be predominantly due to associated production.

X. Acknowledgments

This experiment was made possible by the support of the Neutrino Department at Fermilab and, in particular, the operating crew of the 15-foot bubble chamber. We also wish to thank our scanners at all three institutions for their support. This paper was completed only because of the unfailing cooperation of S. Klepec.

References

1. The flux for the 300 GeV exposure is given in M. Derrick et al., Phys. Rev. Letters 36, 936 (1976).

2. The 400 GeV flux may be found in P. Schreiner, "Neutral Current Interactions in Hydrogen and Deuterium," ANL-HEP-CP-76-43, Proceedings of the 1976 Aachen Neutrino Conference.

3. S. J. Barish et al., "Scaling Variable Distributions in Deep-Inelastic Antineutrino-Proton Interactions," Carnegie-Mellon University Report No. COO-3066-95 (to be published).

4. R. J. Cence et al., Nucl. Instr. and Methods 138, 245 (1976).

5. A. Grant, CERN Report No. CERN/D. Ph. II/Phys. 75-7; S. J. Barish et al., Carnegie-Mellon University Report No. COO-3066-61 (unpublished).

6. S. J. Barish et al., Phys. Letters 66B, 291 (1977).

7. J. W. Chapman et al., Phys. Rev. Letters 36, 124 (1976).

8. P. H. Garbincius et al., Phys. Rev. Letters 32, 328 (1974).

9. A. J. Sadoff et al., Phys. Rev. Letters 32, 955 (1974).

10. J. Ballam et al., Phys. Rev. D5, 545 (1972).

11. The compilation of data in Figs. 6 and 7 is taken from H. Muirhead, Proceedings of the International Symposium on $\bar{p}p$ Interactions, Loma-Koli, Finland, June 1975, p. 300.

12. See Sections VI and VII, respectively.

13. J. W. Chapman et al., Phys. Rev. D14, 14 (1976).

14. P. Schreiner and F. vonHippel, Nucl. Phys. B58, 333 (1973).
D. Perkins, Proceedings of the 1975 International Symposium on Lepton and Photon Interactions (Stanford University), p. 571.

15. G. Wolf, Proceedings of the 1975 International Symposium on Lepton and Photon Interactions (Stanford University), p. 795.

16. P. Bosetti et al., Nucl. Phys. B54, 141 (1973).

17. L. W. Mo, Proceedings of the 1975 International Symposium on Lepton and Photon Interactions (Stanford University), p. 651.

18. C. del Papa et al., Phys. Rev. D15, 15 (1977).

19. T. Kafka et al., ANL-HEP-PR-76-79, Phys. Rev. D (to be published).

20. J. C. Vander Velde, contributed to the IVth International Meeting on Fundamental Physics, Salardu, Spain (1970), University of Michigan preprint.

21. J. C. Vander Velde, contribution to the XII Recontre de Moriand, Flaine, France (1977), University of Michigan preprint.

22. R. D. Field and R. P. Feynman, Phys. Rev. D15, 2590 (1977).

23. L. Sehgal, Nucl. Phys. B90, 471 (1975).

24. A. Seiden, Phys. Letters 68B, 157 (1977).

25. R. P. Feynman, Photon-Hadron Interactions (W. A. Benjamin, New York, 1972); Phys. Rev. Letters 23, 1415 (1969).

26. G. Farrar and J. Rosner, Phys. Rev. D7, 2747 (1973). See also J. L. Newmeyer and D. Sivers, Phys. Rev. D9, 2658 (1974), and S. J. Brodsky and Nathan Weiss, SLAC-PUB-1926 (1977).

28. B. P. Roe, Proceedings of the 1975 International Symposium on Lepton

and Photon Interactions (Stanford University), p. 551.

28. The difference distribution and the distribution for identified protons of Fig. 18(b) do not represent the true Z distribution of the protons since all particles have been assigned the pion mass in calculating the laboratory energy.

29. We note that at an incident energy of about 2 GeV, the strangeness-changing Λ production rate has been measured to be about 2%. T. Eichten et al., Phys. Letters 40B, 593 (1972).

30. H. H. Bingham et al., Phys. Rev. D8, 127 (1973).

31. J. Ballam et al., Phys. Letters 56B, 193 (1975).

32. J. P. Berge et al., Phys. Rev. Letters 36, 127 (1976).

33. F. A. Nezrick, SLAC Summer Institute Talk, October 2-13, 1976.

34. M. K. Gaillard et al., Nucl. Phys. B102, 326 (1976), Erratum Nucl. Phys. B112, 545 (1976).

Table I: Charged Hadronic Multiplicity Distribution as a Function of W

n_C^H / W(GeV)	$0^{(a)}$	2	4	6	8	10	$\langle n_C^H \rangle$	f_2^{--}
	Corrected Numbers of Events							
1.0 - 1.5	23.8	17.4					0.84 ± 0.17	-0.18 ± 0.07
1.5 - 2.0	18.8	52.2	2.3				1.55 ± 0.12	-0.54 ± 0.08
2.0 - 2.5	14.5	49.0	10.3	1.1			1.94 ± 0.15	-0.58 ± 0.09
2.5 - 3.0	10.7	45.7	24.0	1.1			2.38 ± 0.15	-0.75 ± 0.09
3.0 - 3.5	7.5	32.6	30.9	7.8			2.99 ± 0.18	-0.87 ± 0.11
3.5 - 4.0	5.0	28.3	28.6	5.6			3.02 ± 0.18	-0.95 ± 0.11
4.0 - 4.5	2.5	14.1	19.4	8.9	4.1		3.91 ± 0.30	-0.95 ± 0.19
4.5 - 5.0	1.9	9.8	21.7	3.3	2.7		3.74 ± 0.29	-1.09 ± 0.20
5.0 - 10.0	1.9	9.8	27.4	15.6	4.1	5.3	4.81 ± 0.38	-1.06 ± 0.25

[a] Estimated from the Monte Carlo calculation.

Table II: Average Charged Hadronic Multiplicity Versus E_ν for Three W Ranges for ≥ 3-Prongs

$W < 3.0$ GeV

E_ν (GeV)	$\langle n_C^H \rangle$
5 - 10	2.43 ± 0.14
10 - 20	2.35 ± 0.09
20 - 30	2.29 ± 0.11
30 - 40	2.59 ± 0.32
40 - 50	3.52 ± 0.42
50 - 100	2.45 ± 0.28

$3.0 < W < 4.5$ GeV

E_ν (GeV)	$\langle n_C^H \rangle$
10 - 20	3.87 ± 0.22
20 - 30	3.49 ± 0.21
30 - 40	3.27 ± 0.39
40 - 50	3.29 ± 0.30
50 - 100	3.10 ± 0.35

$W > 4.5$ GeV

E_ν (GeV)	$\langle n_C^H \rangle$
20 - 30	4.09 ± 0.41
30 - 40	4.75 ± 0.82
40 - 50	4.63 ± 0.40
50 - 100	4.95 ± 0.53

Table III: $< n_0 >$ Versus Number of Charged Hadrons

	$\bar{\nu} p \to \mu^+ H^o$		$\nu p \to \mu^- H^{++}$[a]
n_C^H	$< n_0 >$ γ Count	$< n_0 >$ $p_\perp$ Method	$< n_0 >$ γ Count
2	0.92 ± 0.16	0.98 ± 0.19	1.5 ± 0.3
4	1.30 ± 0.24	1.39 ± 0.24	2.1 ± 0.3
6	1.81 ± 0.60	1.95 ± 0.44	2.8 ± 0.5
8	1.85 ± 1.1	2.14 ± 0.63	3.2 ± 0.8

[a] See Ref. 13.

Table IV: Strange Particle Events

Observed Strange Particles	No. of Events	Corrected Events[a]	$\frac{\sigma(\bar{\nu} p \to \mu^+ V^o X)}{\sigma(\bar{\nu} p \to \mu^+ H^o)}$[b]
$K_s^o \to \pi^+ \pi^-$	17	74 ± 18	$15 \pm 4\%$
$\Lambda \to p\pi^-$	13	28 ± 8	$6 \pm 2\%$
$K_s^o \to \pi^+ \pi^-$, $K_s^o \to \pi^+ \pi^-$	1	-	-
$K_s^o \to \pi^+ \pi^-$, $\Lambda \to p\pi^-$	1	-	-

[a] Corrected by potential-path weight, for neutral decay modes (including K_L^o) and pass rate.

[b] Inclusive of the two double-Vee events.

Table V: Results of Fitting the Charged-Current Events

Hypothesis	Number of Fits
$\bar{\nu} p \rightarrow \mu^+ p \pi^-$	35
$\bar{\nu} p \rightarrow \mu^+ p \pi^- \pi^+ \pi^-$	12
$\bar{\nu} p \rightarrow \mu^+ p \pi^- 2\pi^+ 2\pi^-$	8
Strange Particle Fits	
$\bar{\nu} p \rightarrow \mu^+ p K^- \pi^+ \pi^- K_s^o$	1
$\bar{\nu} p \rightarrow \mu^+ p \pi^- \pi^+ \pi^- K_s^o K_s^o$	1

Figure Captions

Fig. 1 Definition of the kinematic variables used in the paper.

Fig. 2 (a) Observed distribution in hadronic mass W for $\bar{\nu}p$ CC events. (b) Observed distribution in the four-momentum transfer Q^2 for $\bar{\nu}p$-proton CC events. Both distributions are given for events with three- or more charged tracks.

Fig. 3 The mean of the charged hadronic multiplicity distribution $< n_C^H >$ as a function of Q^2 for events with three- or more charged tracks.

Fig. 4 The charged-hadronic multiplicity distribution for different W selections. The $n_C^H = 0$ values are Monte Carlo estimates.

Fig. 5 The mean-charged hadronic multiplicity $< n_C^H >$ as a function of W^2. A Monte Carlo estimate of 1-prongs is included. For comparison, data from neutrino interactions, photoproduction, and electroproduction are also plotted. The dashed-dotted line is a fit to the neutrino data shown as open circles. The full line is the fit to the $\bar{\nu}p$ data of the present experiment shown as the filled circles.

Fig. 6 Comparison of the mean number of negative hadrons $< n_- >$ as a function of the square of the hadronic mass (W^2) for various reactions. A Monte Carlo estimate of 1-prongs is included for the antineutrino decks. The compilation of annihilation and pp data is taken from Ref. 11. The dashed lines are drawn to guide the eye.

Fig. 7 Multiplicity moment f_2^{--} versus $< n_- >$ for various reactions. A Monte Carlo estimate of 1-prongs is included for the antineutrino decks. All the data except the $\bar{\nu}p$ results of the present experiment are taken from Ref. 11. The pp data and $\bar{p}p$ non-annihilation data are not distinguished. The line which shows the trend of the annihilation data is also parallel to the $\bar{\nu}p$ results.

Fig. 8 Mean number of neutral pions, $\langle n_0 \rangle$ as a function of the number of negative tracks, n_-, as determined by the two independent methods described in the text. The line is the best fit to the data.

Fig. 9 (a) $F_2(Y_R) = \frac{1}{N_T} \frac{1}{\pi} \frac{dN}{dY_R}$ versus rapidity, Y_R, for π^-, π^+ and identified proton production. (b) $F_1(X_F) = \frac{1}{N_T} \frac{2}{\pi\sqrt{s}} \int_0^\infty E^* \frac{d^2N}{dX_F dp_\perp^2} dp_\perp^2$ versus Feynman X_F for π^-, π^+ and identified proton production. The lines are fits to the combined π^+ and π^- data.

Fig. 10 $F_1(X_F) = \frac{1}{N_T} \frac{2}{\pi\sqrt{s}} \int_0^\infty E^* \frac{d^2N}{dX_F dp_\perp^2} dp_\perp^2$ versus Feynman X_F for pion production in antineutrino-proton interactions compared with similar pion production data from the interactions of real and virtual photons. The $\bar{\nu}p$ data is approximately normalized to the e^-p data for $X_F < 0$.

Fig. 11 $F_1(X_F) = \frac{1}{N_T} \frac{2}{\pi\sqrt{s}} \int_0^\infty E^* \frac{d^2N}{dX_F dp_\perp^2} dp_\perp^2$ versus Feynman X_F for $\bar{\nu}p$ interactions compared with the distribution for the hadronic reaction $\pi^+p \rightarrow \pi^-X$ at 8 GeV/c. The hadronic data is taken from Ref. 16 and is normalized to agree with the $\bar{\nu}p$ data ignoring the points near $X_F = 0$.

Fig. 12 Normalized transverse momentum distribution of hadrons with respect to the axis of the total hadronic system. The line represents the best fit to the data over the range $0.04 < p_\perp^2 < 1.2$ $(GeV/c)^2$.

Fig. 13 Average $p_\perp$ as a function of (a) X_F and (b) Y_R for $\bar{\nu}p$ and νp data. The latter have the W selections noted.

Fig. 14 Normalized Z distribution for charged hadrons as a function of incident antineutrino energy. The variable N_E is the number of events in the three $\bar{\nu}$ energy intervals noted. Scaling is observed for $Z \gtrsim 0.3$.

Fig. 15 Normalized Z distribution for π^- production in $\bar{\nu}p$ CC interactions; the curves are predictions by Field and Feynman (Ref. 22), Sehgal (Rev. 23) and Seiden (Ref. 24).

Fig. 16 Charged hadron ratio for $Z \geq 0.2$ as a function of (a) X, (b) Y, (c) Q^2, and (d) W. No obvious thresholds are apparent although the ratio falls as W and Y are increased.

Fig. 17 Average transverse momentum $\langle p_\perp \rangle$ versus (a) X, (b) Z, (c) Q^2, and (d) W^2 for $\bar{\nu}p$, νp, and $\mu^+ p$ data.

Fig. 18 Charge distributions for $\bar{\nu}p$ and νp CC interactions as a function of Y_R. The dotted lines show the average charge over the range of Y_R covered by the lines. Although the mean charges do not plateau at the simple values expected from the quark fragmentation pictures shown in the inserts, there is an indication of a lower mean charge in the current fragmentation region, $Y_R > 0$, as compared to the target fragmentation region $Y_R < 0$.

Fig. 19 Uncorrected Z distributions for (a) $\bar{\nu}p \rightarrow \mu^+ \pi^- X$ and $\nu p \rightarrow \mu^- \pi^+ X$, (b) difference of the two Z distributions in (a). The open data points in (b) are the observed proton data. The curves are hand-drawn to guide the eye.

Fig. 20 Relative rate of visible V^0 production as a function of W in various reactions.

Fig. 21 Uncorrected inclusive Q^2, $E_{\bar{\nu}}$, X, Y and W distributions for all $\bar{\nu}p \to \mu^+$ events and for those with visible strange particles.

Fig. 22 The rapidity and $p_\perp^2$ distributions for the observed K^o and Λ particles.

Fig. 23 Distribution of invariant mass and four-momentum transfer in the exclusive reaction $\bar{\nu}p \to \mu^+ p \pi^-$.

(a)

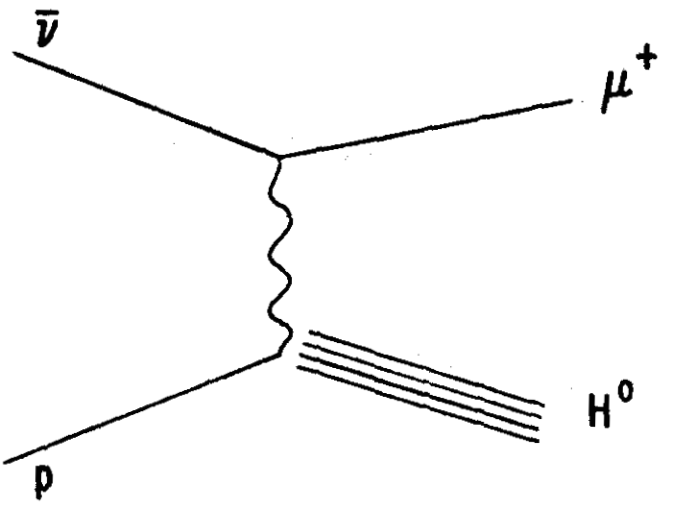

q = 4 MOMENTUM TRANSFER

p = TARGET 4 MOMENTUM

M = PROTON MASS

$E_{\bar{\nu}}$ = ANTI-NEUTRINO ENERGY

h = 4 MOMENTUM OF A HADRON

$\nu = p.q$

$X = q^2 / 2M\nu$

$Y = \nu / E_{\bar{\nu}}$

$Z = h.p / p.q$

(b)

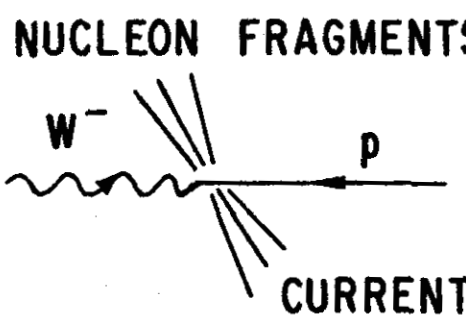

$\sqrt{S}$ = c.m. ENERGY

$$X_F = 2 p_{||} / \sqrt{S}$$

$$Y_R = 1/2 \ln \left((E + p_{||}) / (E - p_{||}) \right)$$

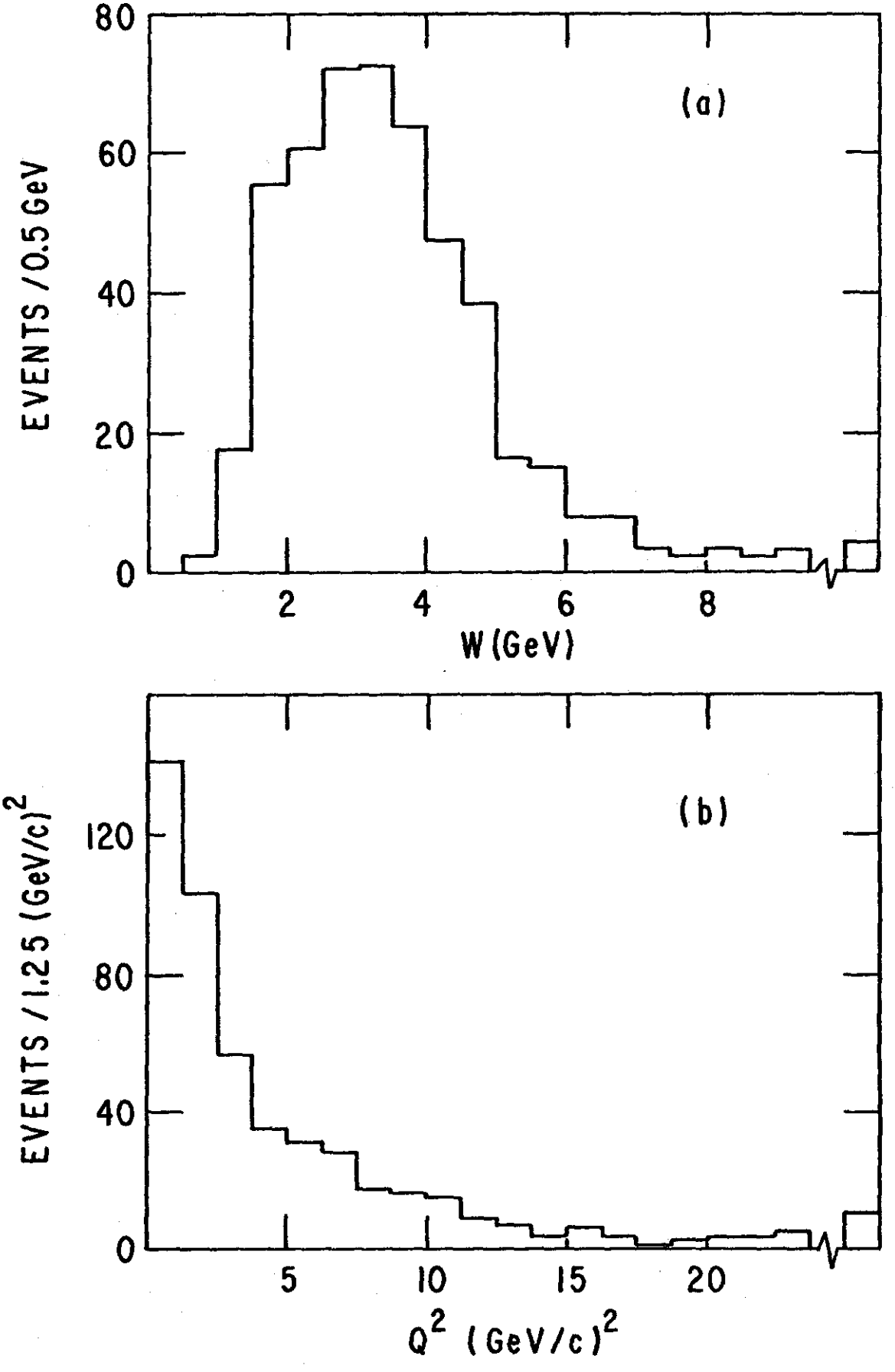
80
60
40
20
0
EVENTS /0.5 GeV
(a)
2
4
6
8
W (GeV)
120
80
40
0
EVENTS / 1.25 (GeV/c)^2
(b)
5
10
15
20
Q^2 (GeV/c)^2

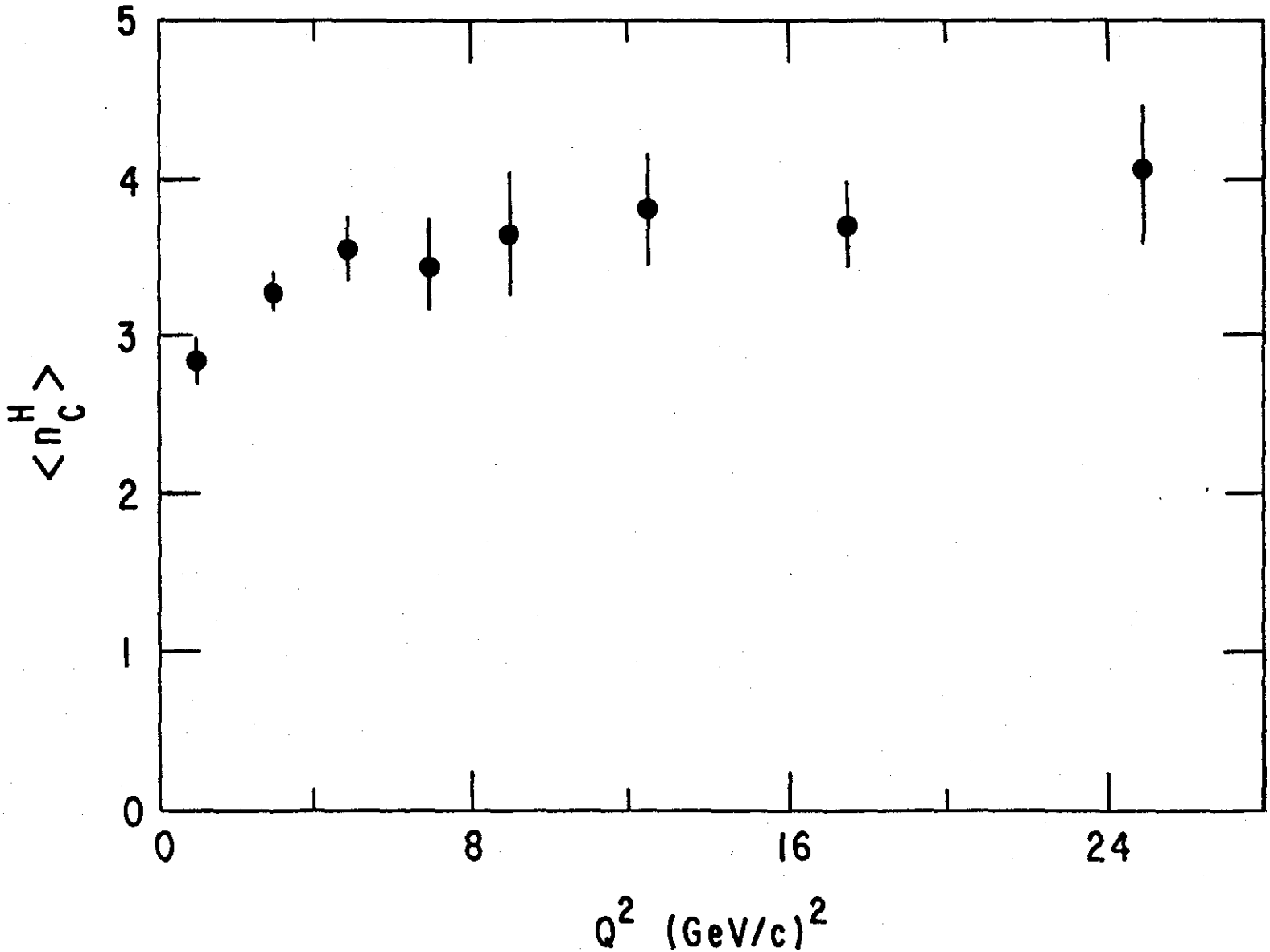
5
4
3
2
1
0
0
8
16
24
$\langle n_c^H \rangle$
Q^2 (GeV/c)^2

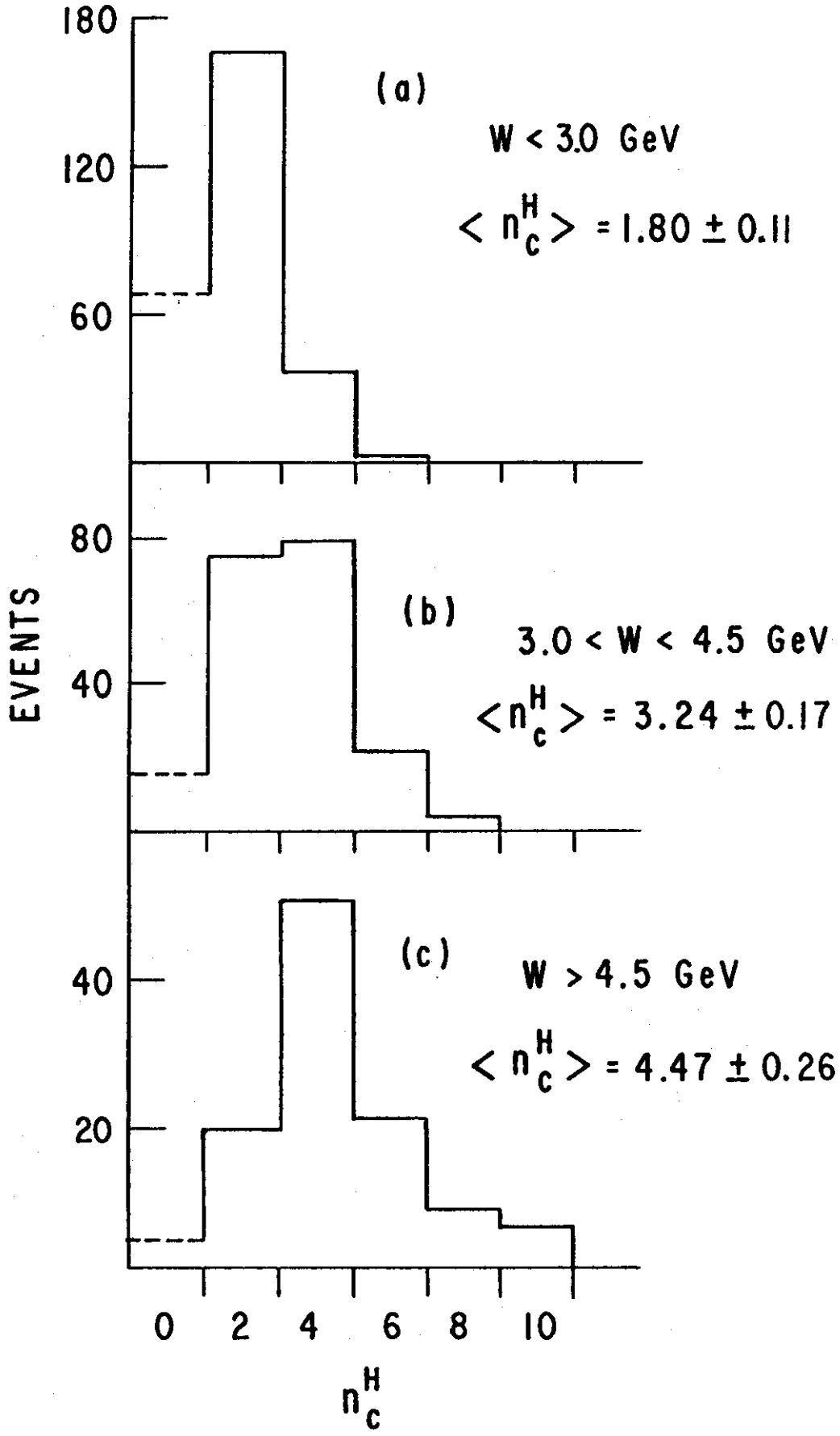
180
120
60
(a)
W < 3.0 GeV
$\langle n_c^H \rangle = 1.80 \pm 0.11$
80
40
(b)
3.0 < W < 4.5 GeV
$\langle n_c^H \rangle = 3.24 \pm 0.17$
EVENTS
40
20
(c)
W > 4.5 GeV
$\langle n_c^H \rangle = 4.47 \pm 0.26$
0
2
4
6
8
10
n_c^H

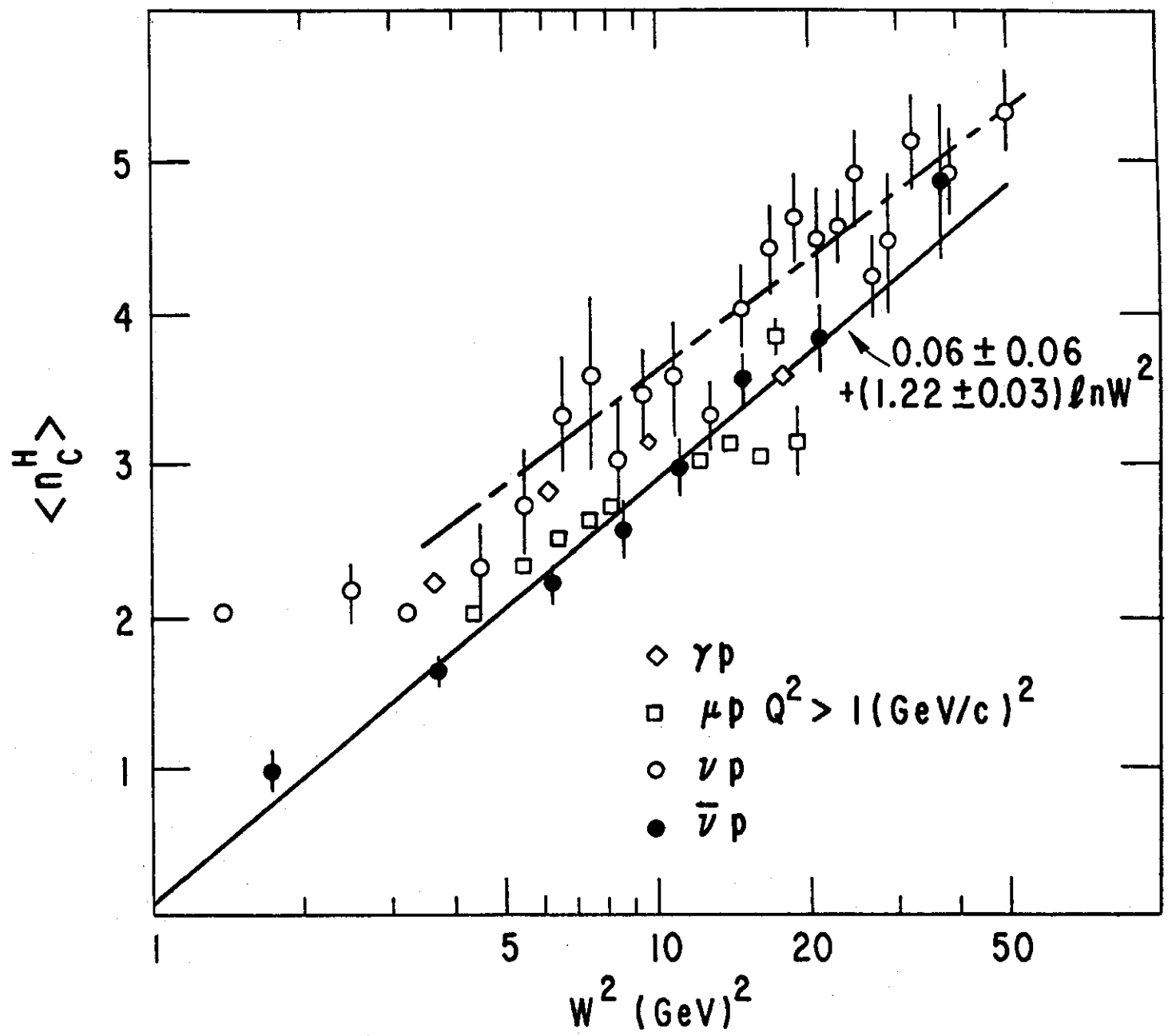
$\langle n_c^H \rangle$
5
4
3
2
1
1
5
10
20
50
W^2 (GeV)^2
$0.06 \pm 0.06 + (1.22 \pm 0.03) \ell n W^2$
γp
μp $Q^2 > 1$ (GeV/c)^2
νp
$\bar{\nu} p$

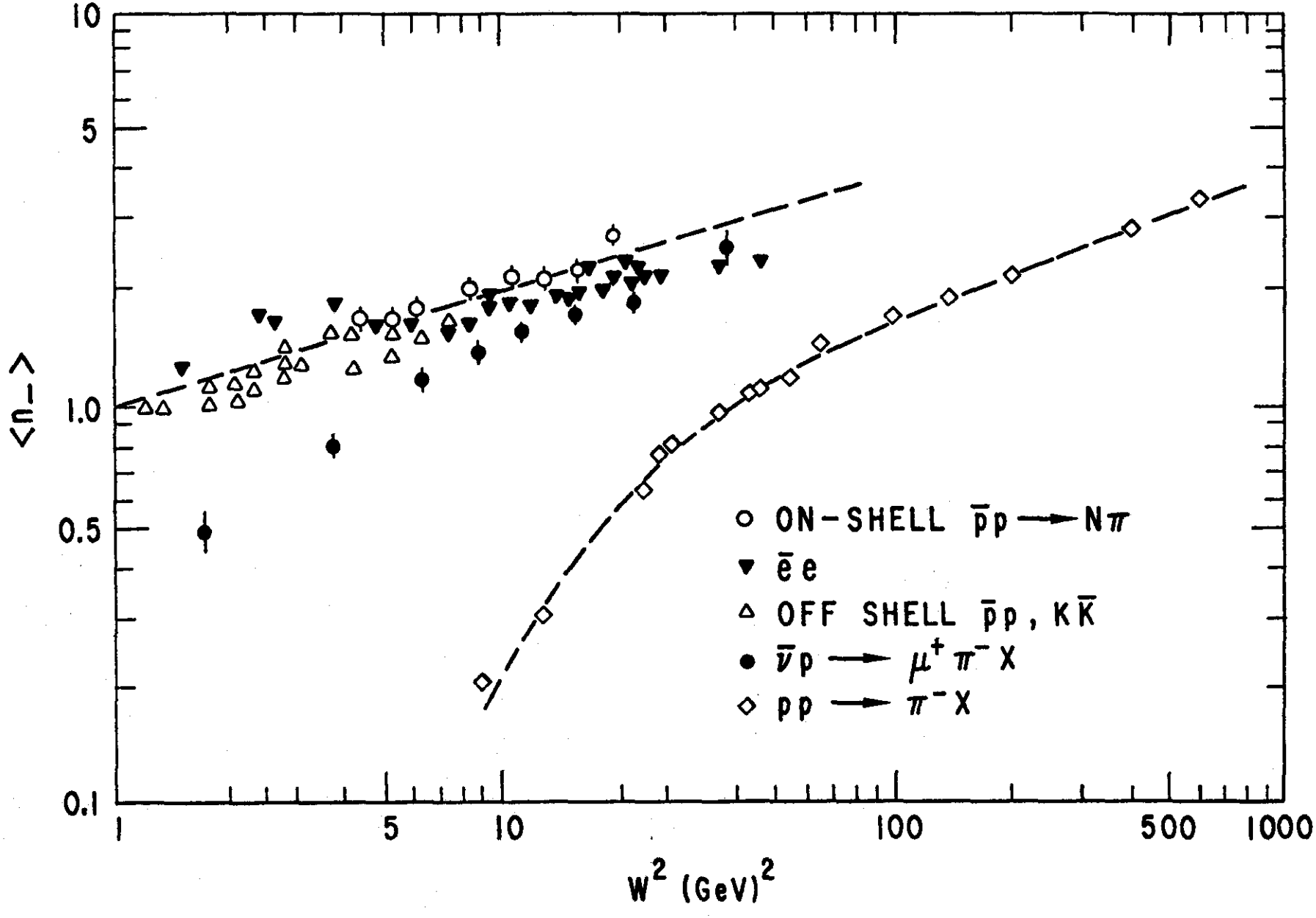
10
5
1.0
0.5
0.1
$\langle n_- \rangle$
1
5
10
100
500
1000
W^2 (GeV)^2
ON-SHELL $\bar{p}p \rightarrow N\pi$
$\bar{e}e$
OFF SHELL $\bar{p}p$, $K\bar{K}$
$\bar{\nu}p \rightarrow \mu^+\pi^-X$
$pp \rightarrow \pi^-X$

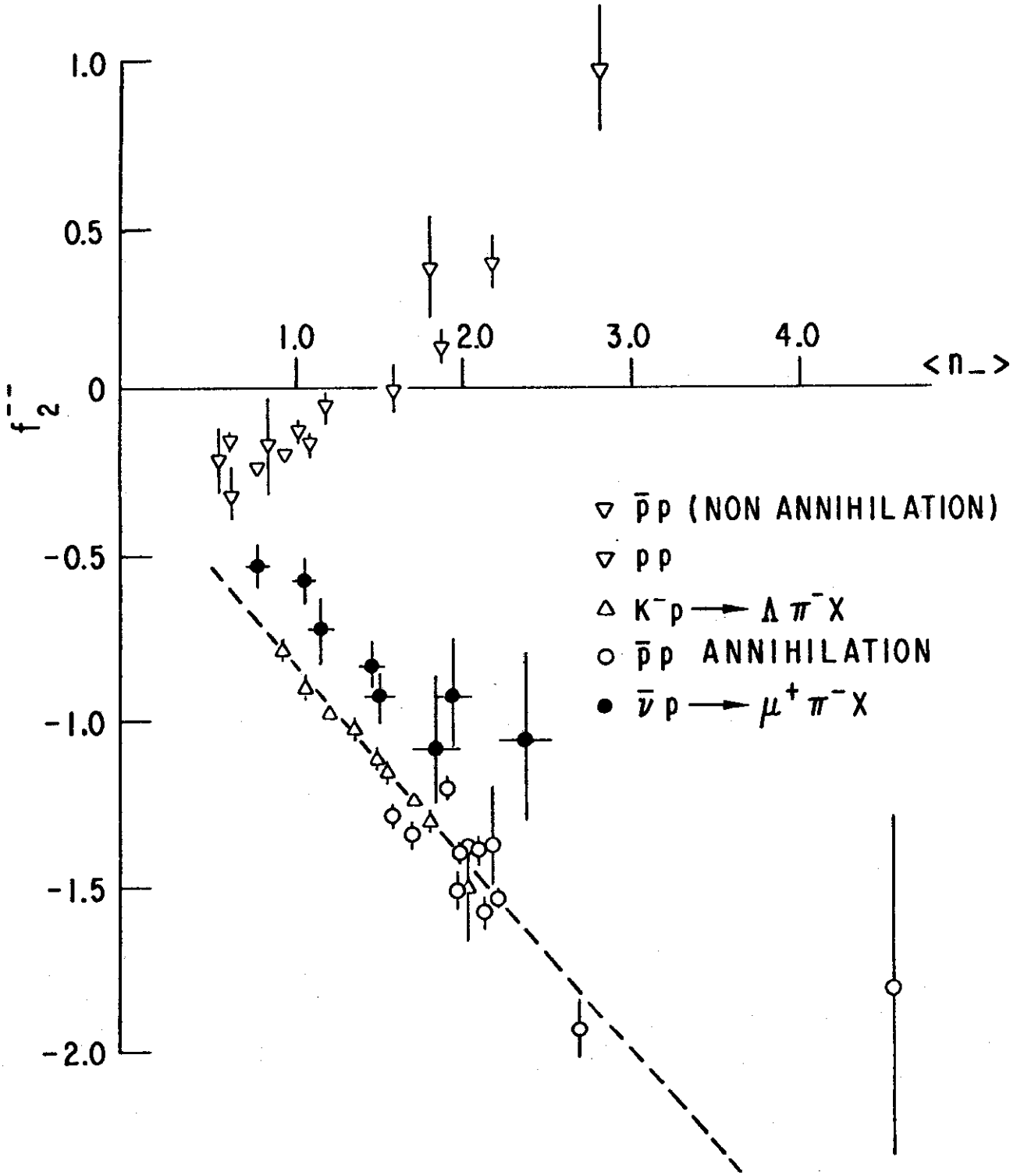
1.0
0.5
0
-0.5
-1.0
-1.5
-2.0
1.0
2.0
3.0
4.0
<n_>
f_2^--
p̄p (NON ANNIHILATION)
pp
K⁻p → Λ π⁻X
p̄p ANNIHILATION
ν̄p → μ⁺π⁻X

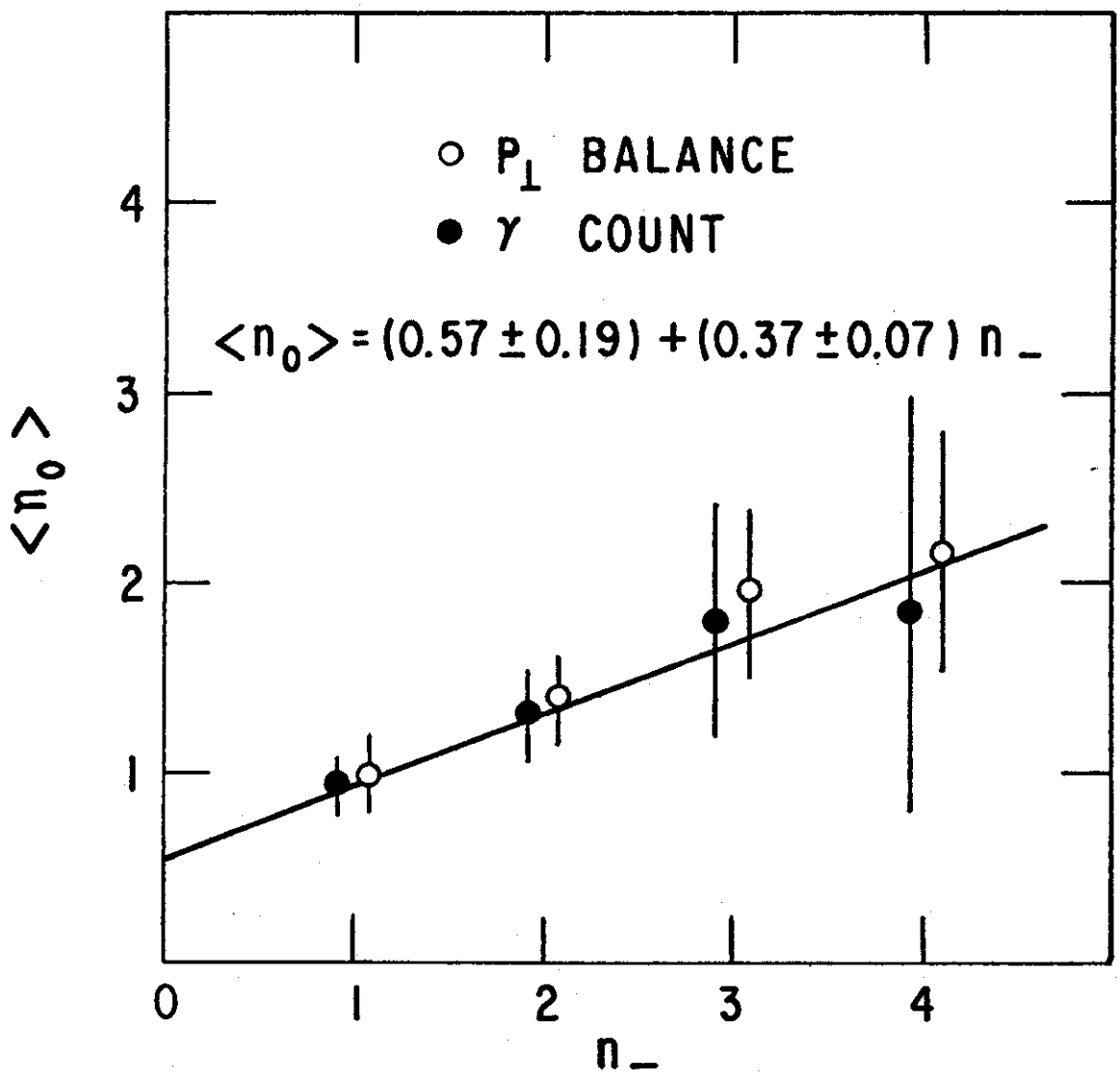
○ $P_\perp$ BALANCE
● γ COUNT
$\langle n_0 \rangle = (0.57 \pm 0.19) + (0.37 \pm 0.07)\, n_-$
$\langle n_0 \rangle$
n_-
0
1
2
3
4

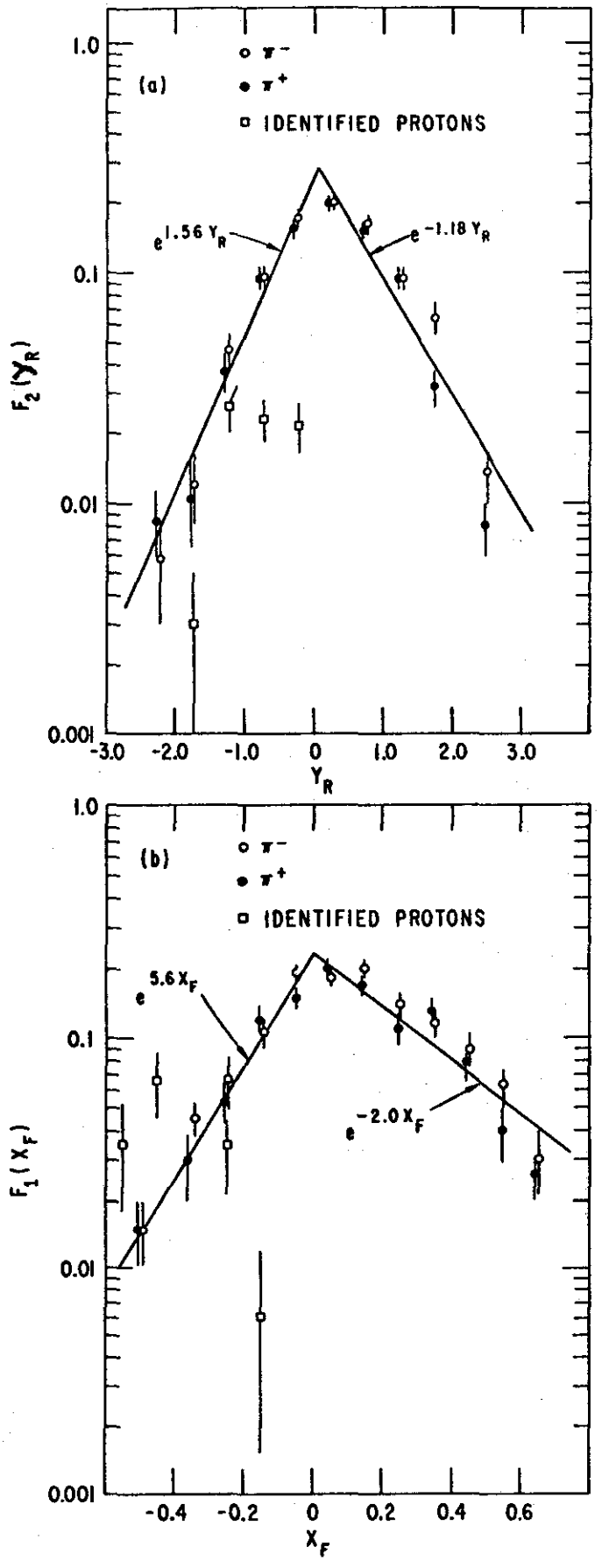
(a)
π⁻
π⁺
IDENTIFIED PROTONS
e^1.56 Y_R
e^-1.18 Y_R
F_2(Y_R)
1.0
0.1
0.01
0.001
-3.0
-2.0
-1.0
0
1.0
2.0
3.0
Y_R
(b)
π⁻
π⁺
IDENTIFIED PROTONS
e^5.6 X_F
e^-2.0 X_F
F_1(X_F)
1.0
0.1
0.01
0.001
-0.4
-0.2
0
0.2
0.4
0.6
X_F

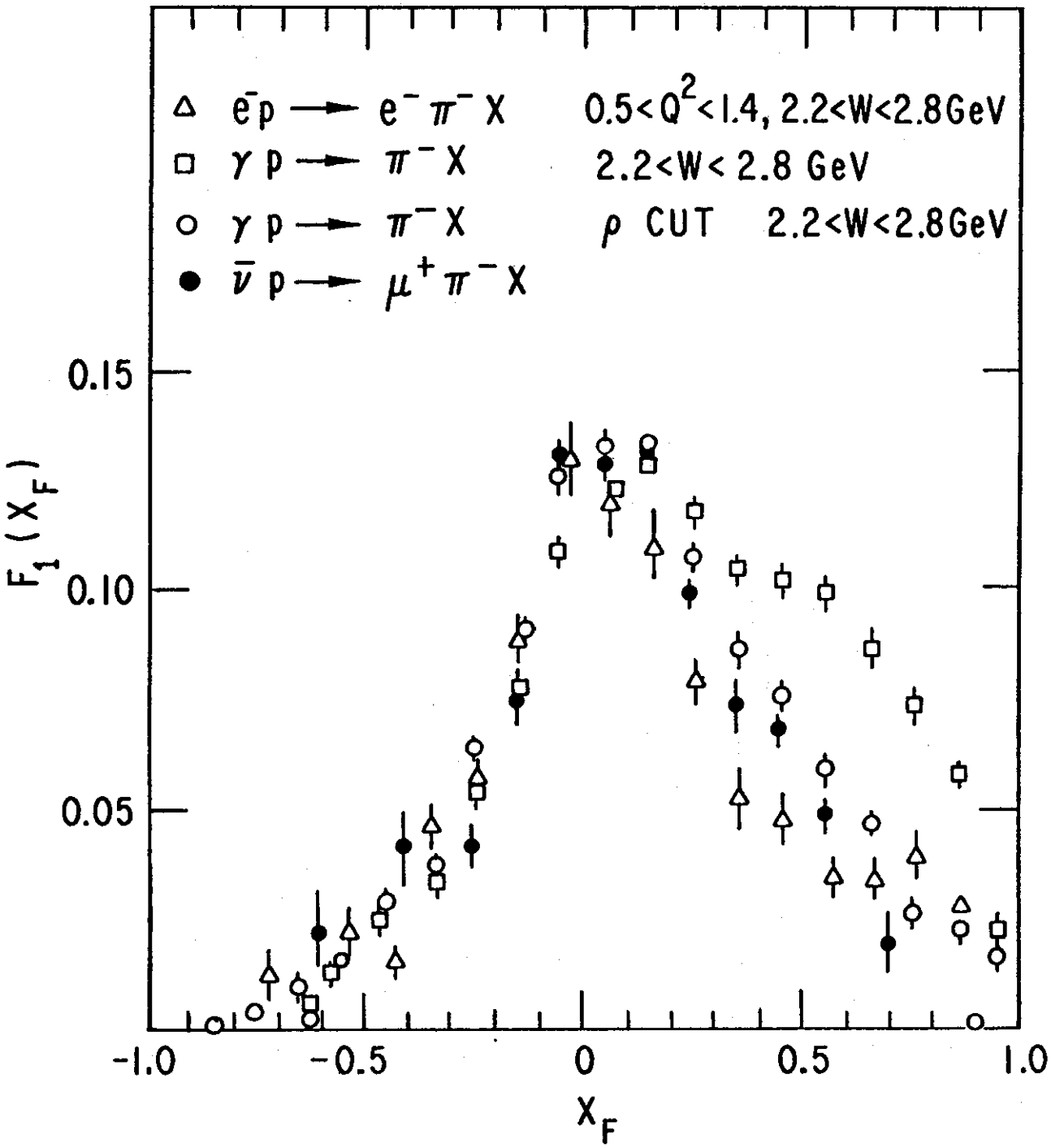
△ e⁻p → e⁻π⁻X 0.5<Q²<1.4, 2.2<W<2.8GeV
□ γp → π⁻X 2.2<W<2.8 GeV
○ γp → π⁻X ρ CUT 2.2<W<2.8GeV
● ν̄p → μ⁺π⁻X
0.15
0.10
0.05
F₁(X_F)
-1.0
-0.5
0
0.5
1.0
X_F

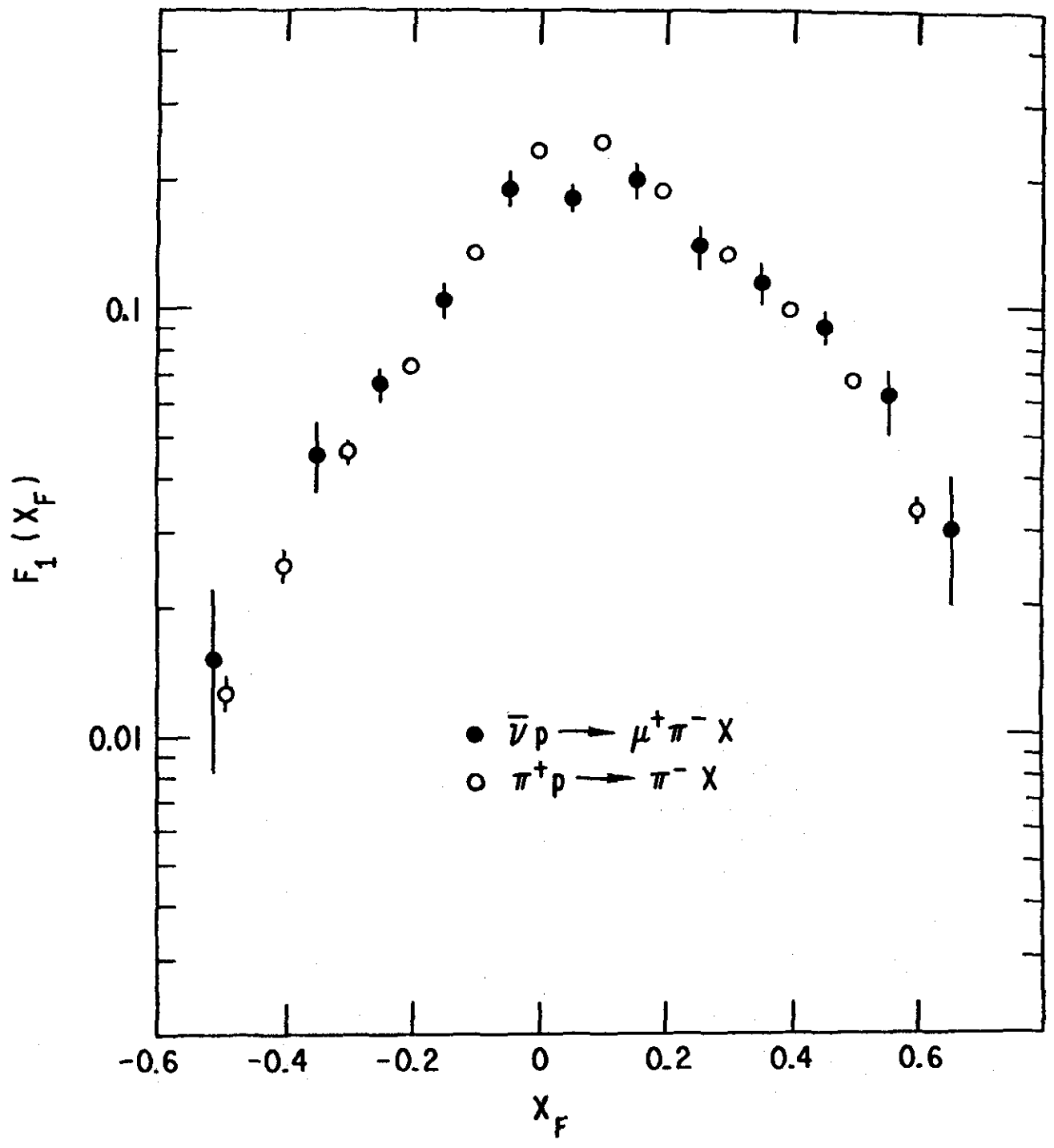
0.1
0.01
$F_1(X_F)$
$\bar{\nu} p \rightarrow \mu^+ \pi^- X$
$\pi^+ p \rightarrow \pi^- X$
-0.6
-0.4
-0.2
0
0.2
0.4
0.6
X_F

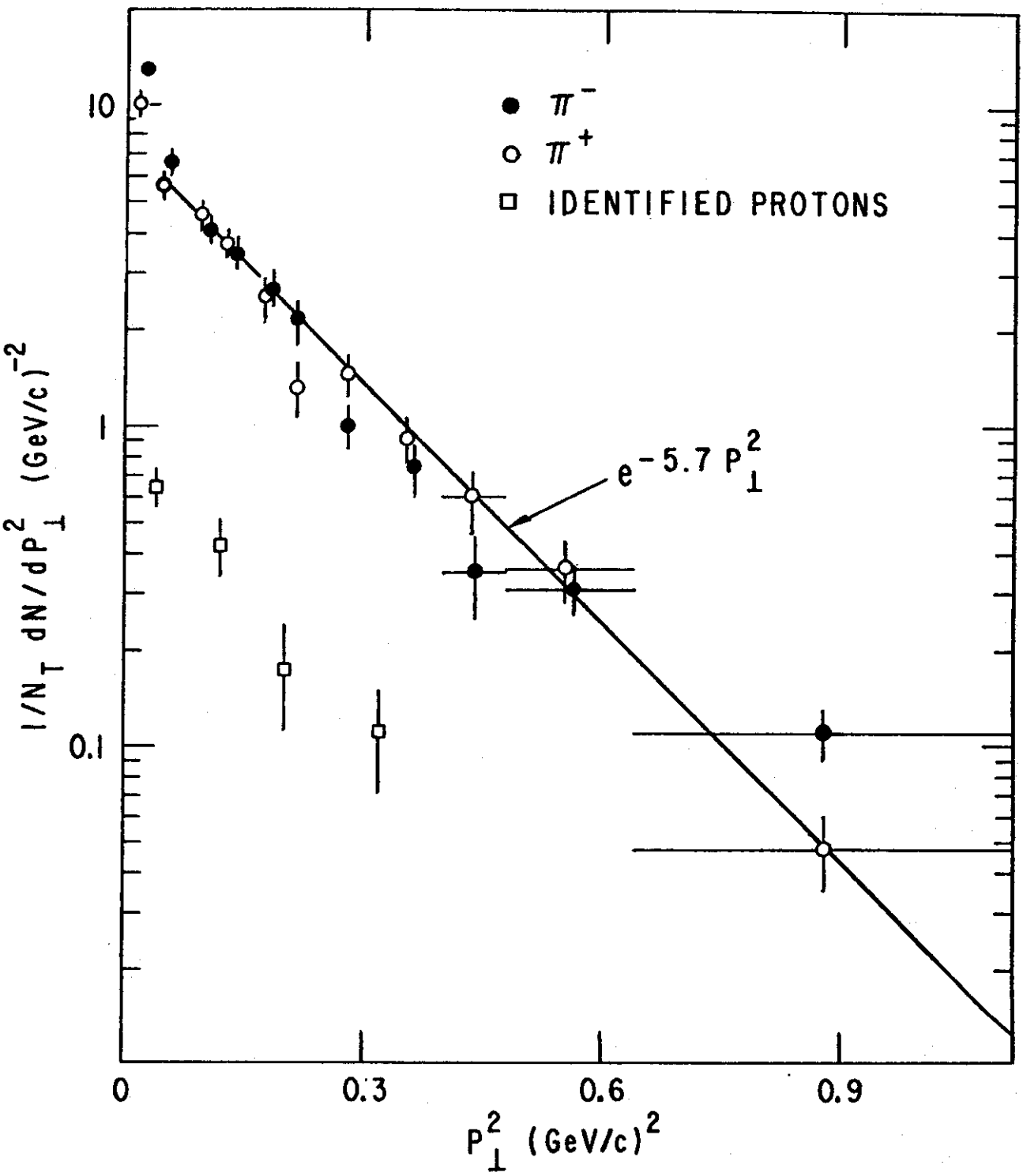
10
1
0.1
0
0.3
0.6
0.9
π^-
π^+
IDENTIFIED PROTONS
$e^{-5.7\,P_\perp^2}$
$1/N_T\ dN/dP_\perp^2\ (GeV/c)^{-2}$
$P_\perp^2\ (GeV/c)^2$

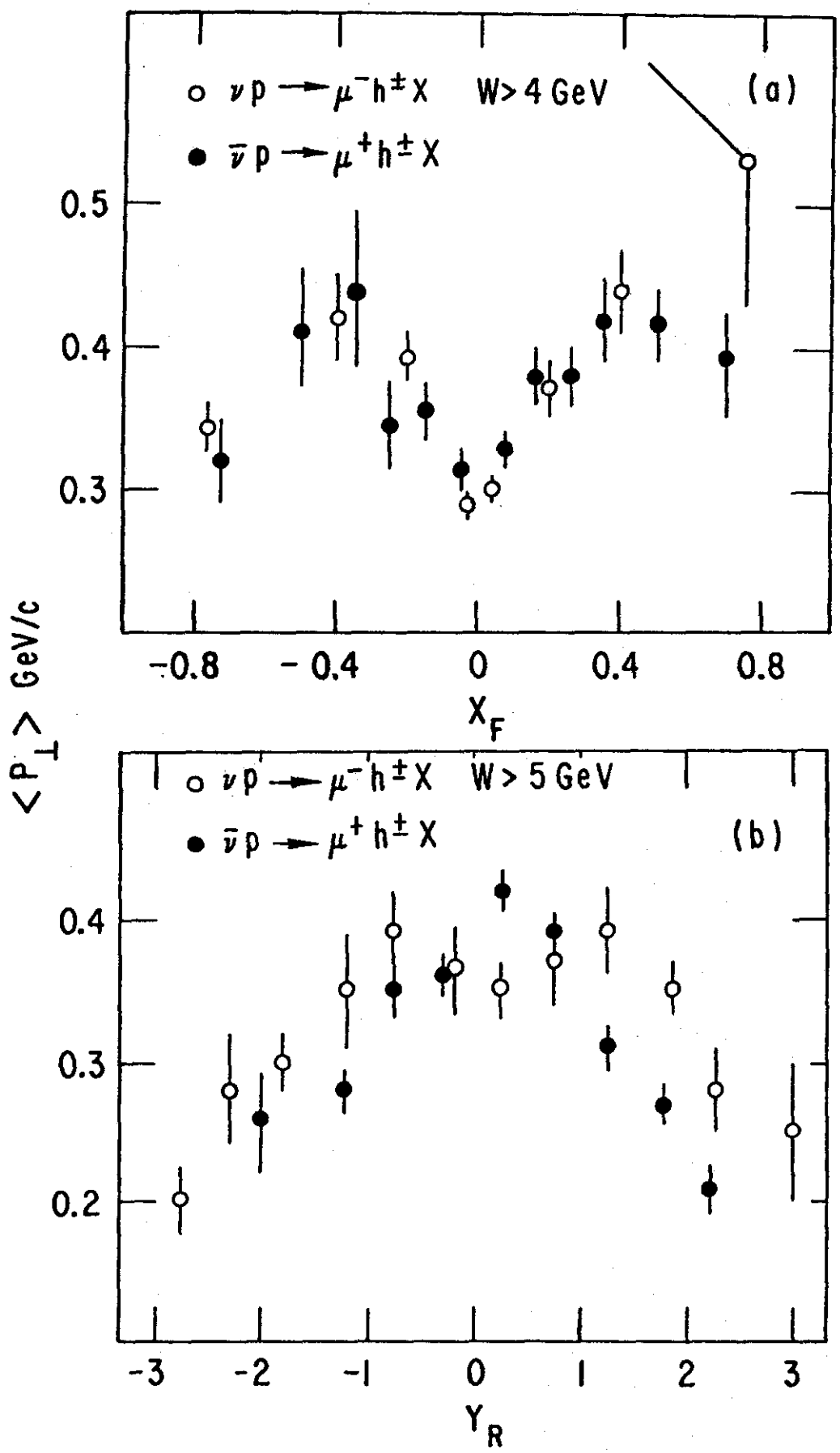
o νp → μ⁻h±X W>4 GeV
(a)
● ν̄p → μ⁺h±X
0.5
0.4
0.3
-0.8
-0.4
0
0.4
0.8
X_F
<P_T> GeV/c
o νp → μ⁻h±X W>5 GeV
● ν̄p → μ⁺h±X
(b)
0.4
0.3
0.2
-3
-2
-1
0
1
2
3
Y_R

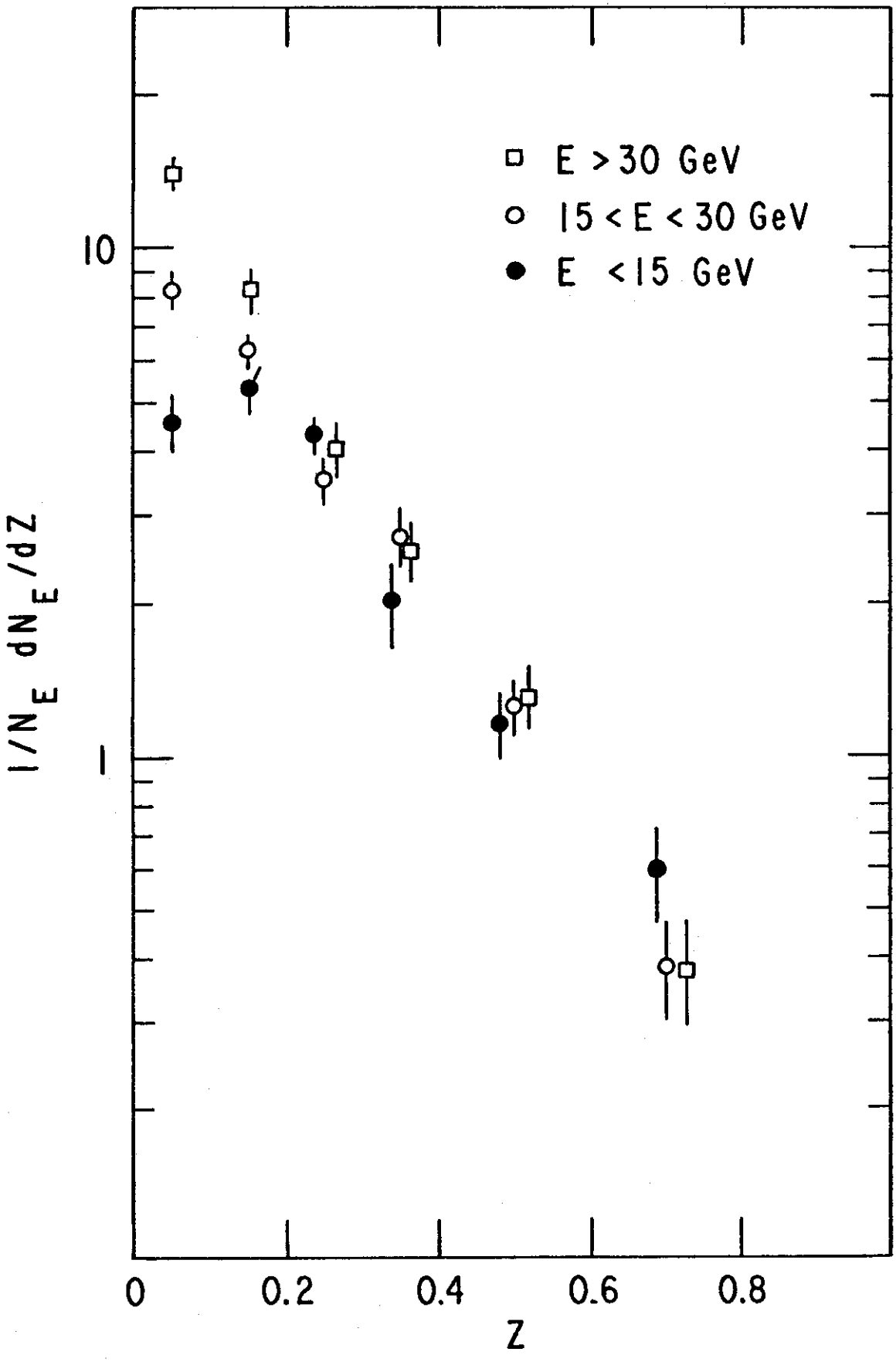
E > 30 GeV
15 < E < 30 GeV
E < 15 GeV
10
1
$1/N_E \; dN_E/dZ$
0
0.2
0.4
0.6
0.8
Z

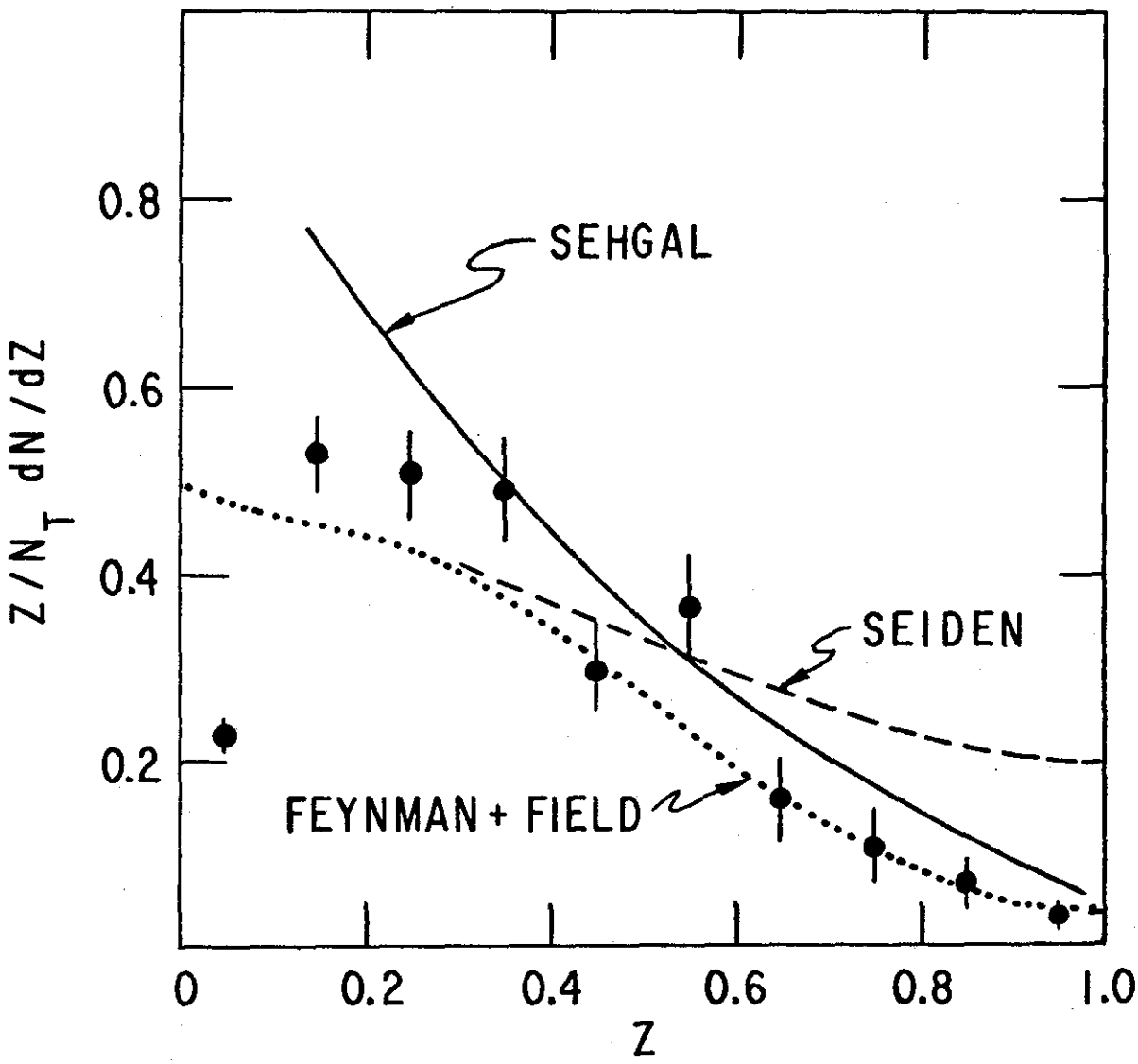
0.8
0.6
0.4
0.2
$Z/N_T\ dN/dZ$
SEHGAL
SEIDEN
FEYNMAN + FIELD
0
0.2
0.4
0.6
0.8
1.0
Z

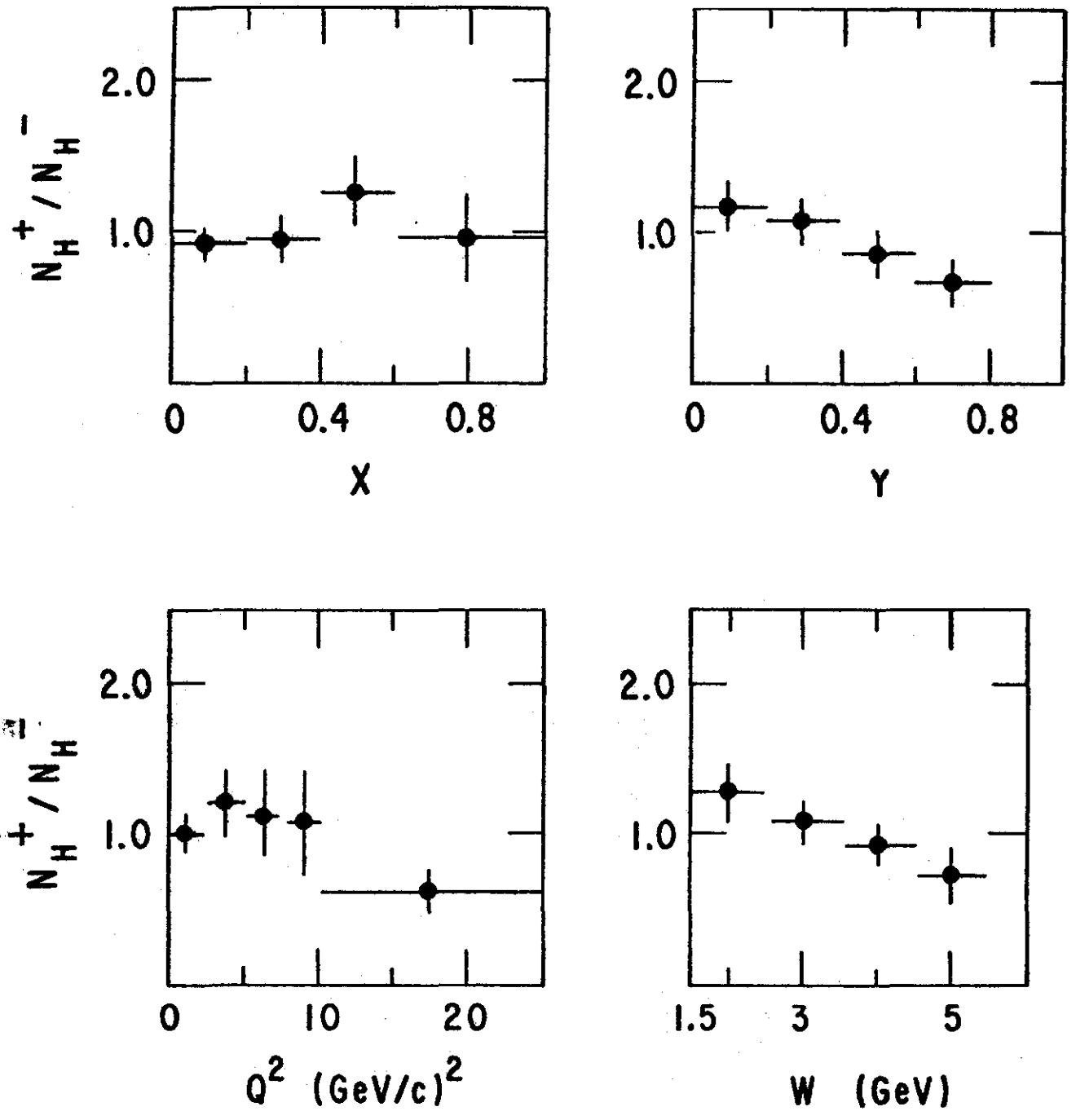
2.0
1.0
N_H^+ / N_H^-
0
0.4
0.8
X
Y
Q^2 (GeV/c)^2
W (GeV)
10
20
1.5
3
5

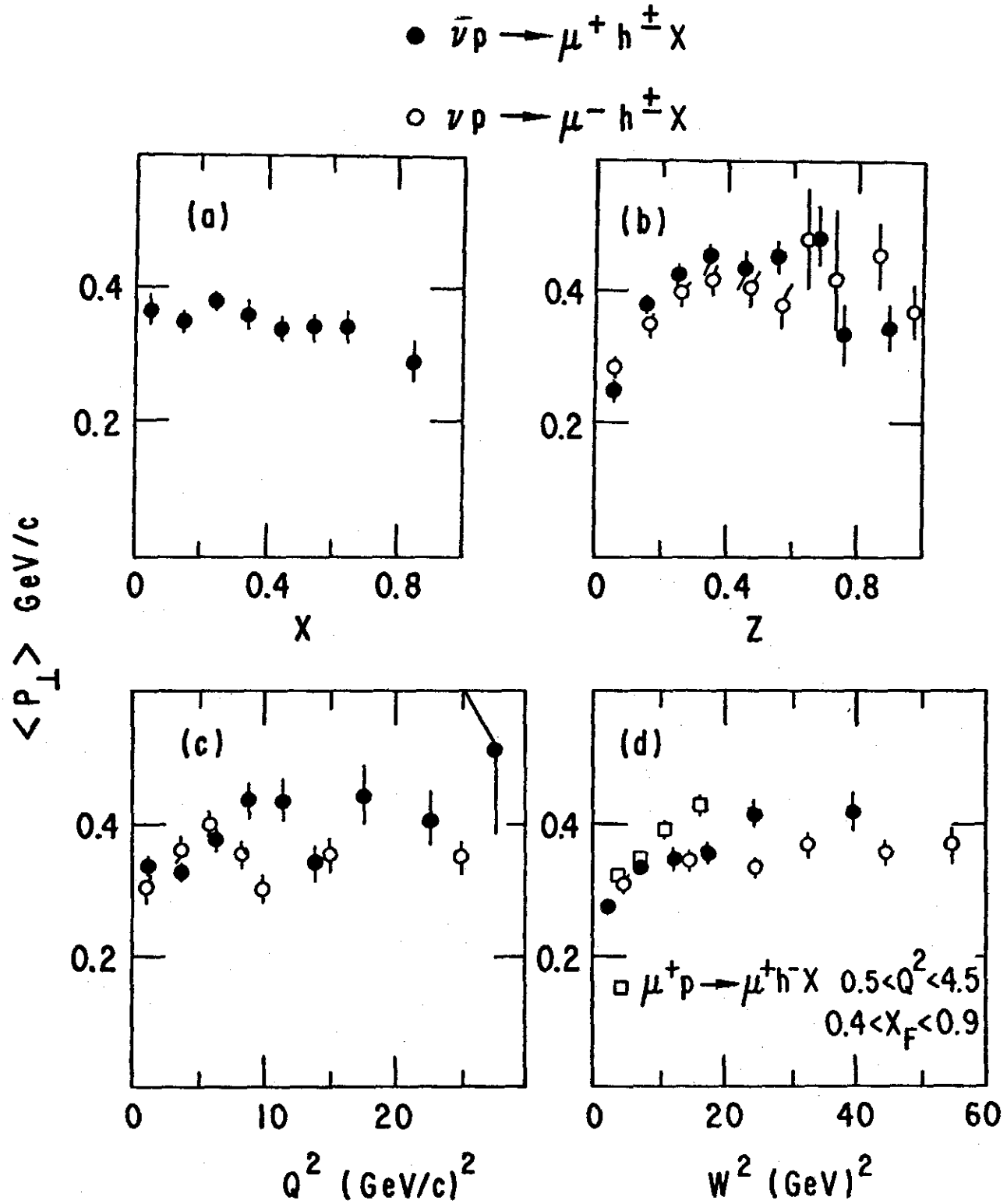
● $\bar{\nu} p \rightarrow \mu^+ h^\pm X$
○ $\nu p \rightarrow \mu^- h^\pm X$
(a)
(b)
(c)
(d)
$\langle P_T \rangle$ GeV/c
0.4
0.2
0
0.4
0.8
X
Z
10
20
40
60
Q^2 (GeV/c)^2
W^2 (GeV)^2
□ $\mu^+ p \rightarrow \mu^+ h^- X$ $0.5 < Q^2 < 4.5$
$0.4 < X_F < 0.9$

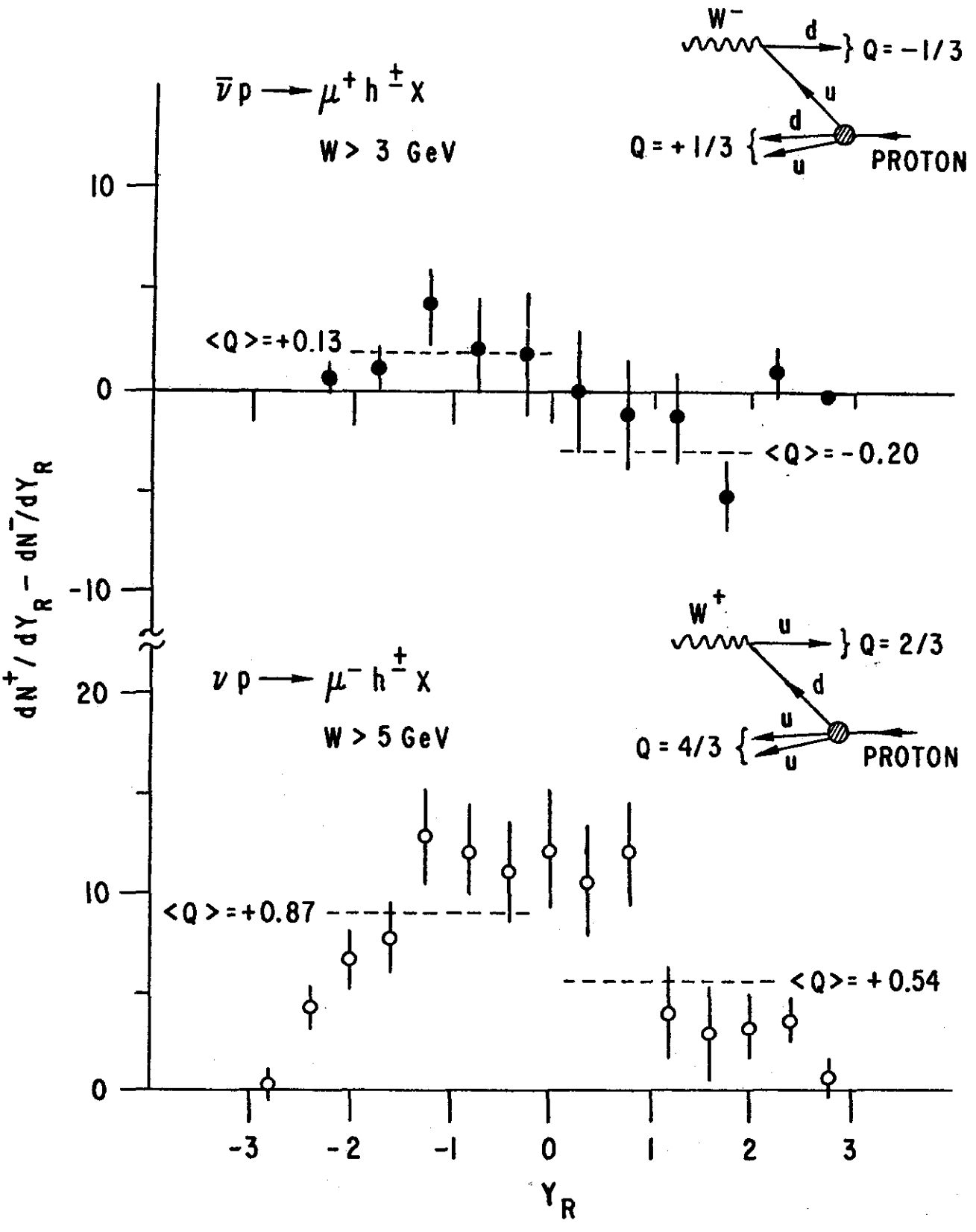
$\bar{\nu} p \rightarrow \mu^+ h^\pm X$
W > 3 GeV
W⁻
d
Q = −1/3
u
d
Q = +1/3
u
PROTON
10
0
−10
<Q> = +0.13
<Q> = −0.20
$dN^+/dY_R - dN^-/dY_R$
$\nu p \rightarrow \mu^- h^\pm X$
W > 5 GeV
W⁺
u
Q = 2/3
d
u
Q = 4/3
u
PROTON
20
10
0
<Q> = +0.87
<Q> = +0.54
−3
−2
−1
0
1
2
3
Y_R

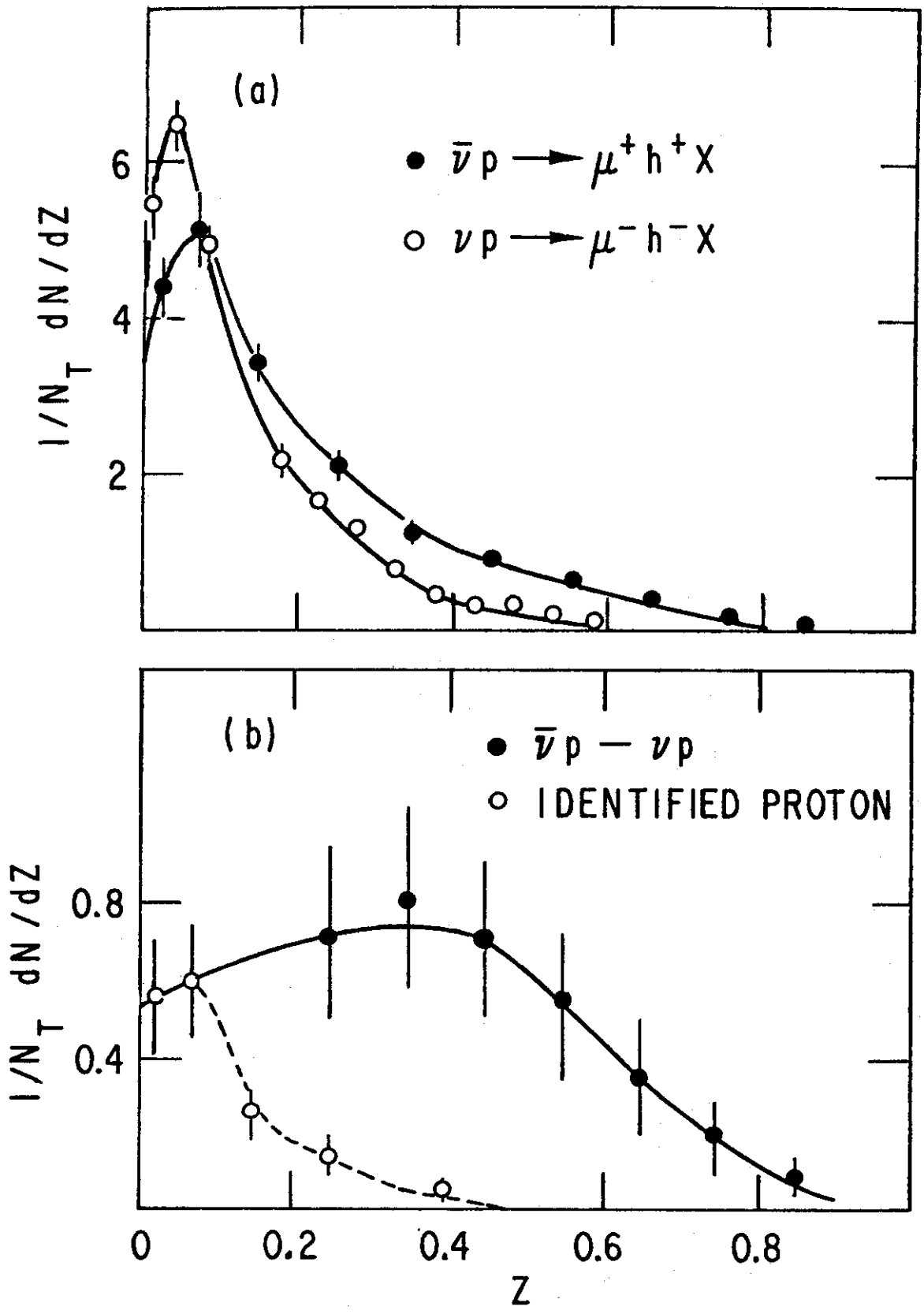
(a)
$\bar{\nu}p \rightarrow \mu^+ h^+ X$
$\nu p \rightarrow \mu^- h^- X$
$1/N_T \; dN/dZ$
6
4
2
(b)
$\bar{\nu}p - \nu p$
IDENTIFIED PROTON
$1/N_T \; dN/dZ$
0.8
0.4
0
0.2
0.4
0.6
0.8
Z

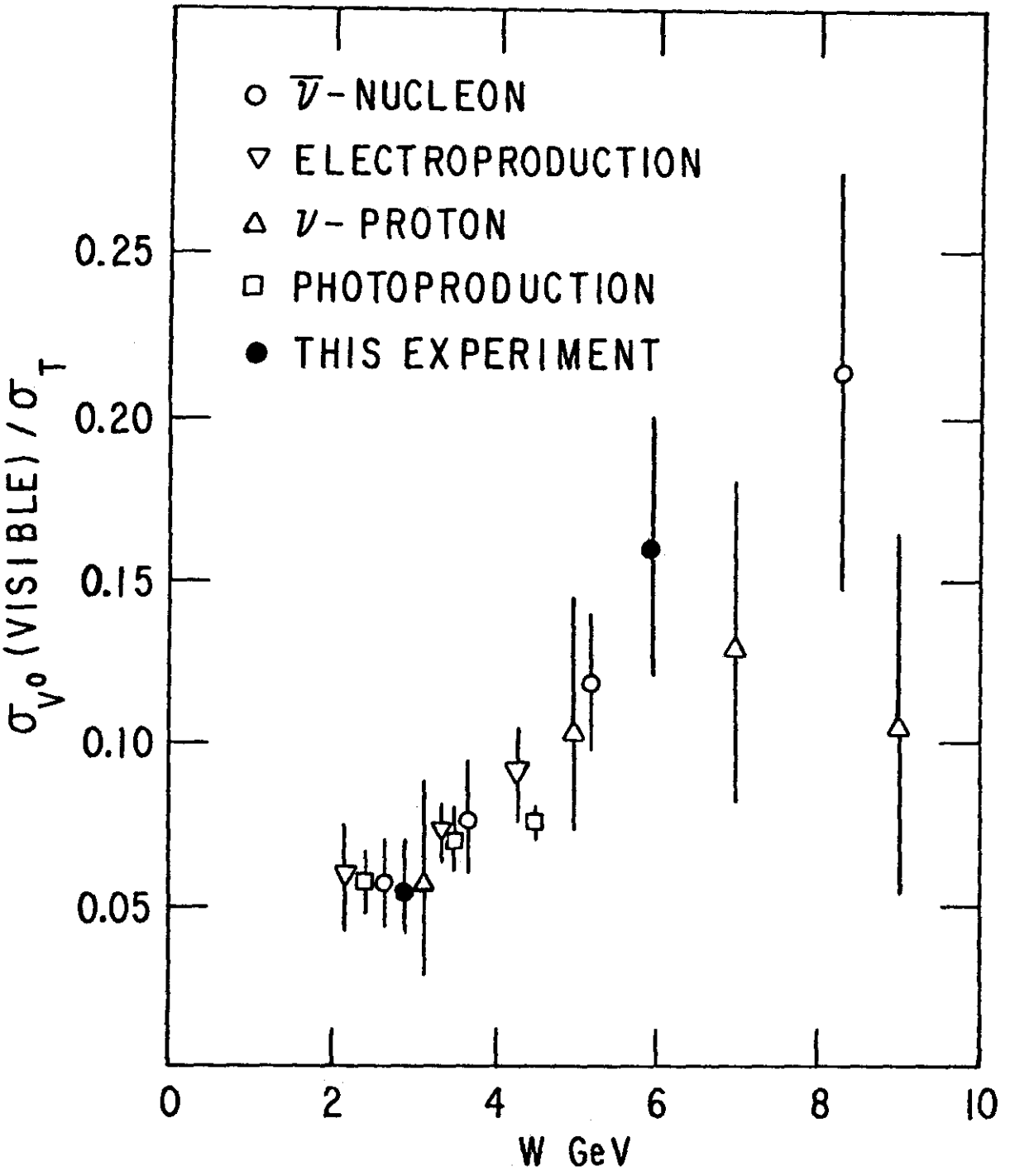
$\bar{\nu}$-NUCLEON
ELECTROPRODUCTION
ν-PROTON
PHOTOPRODUCTION
THIS EXPERIMENT
σ_{V^0} (VISIBLE) / σ_T
0.25
0.20
0.15
0.10
0.05
0
2
4
6
8
10
W GeV

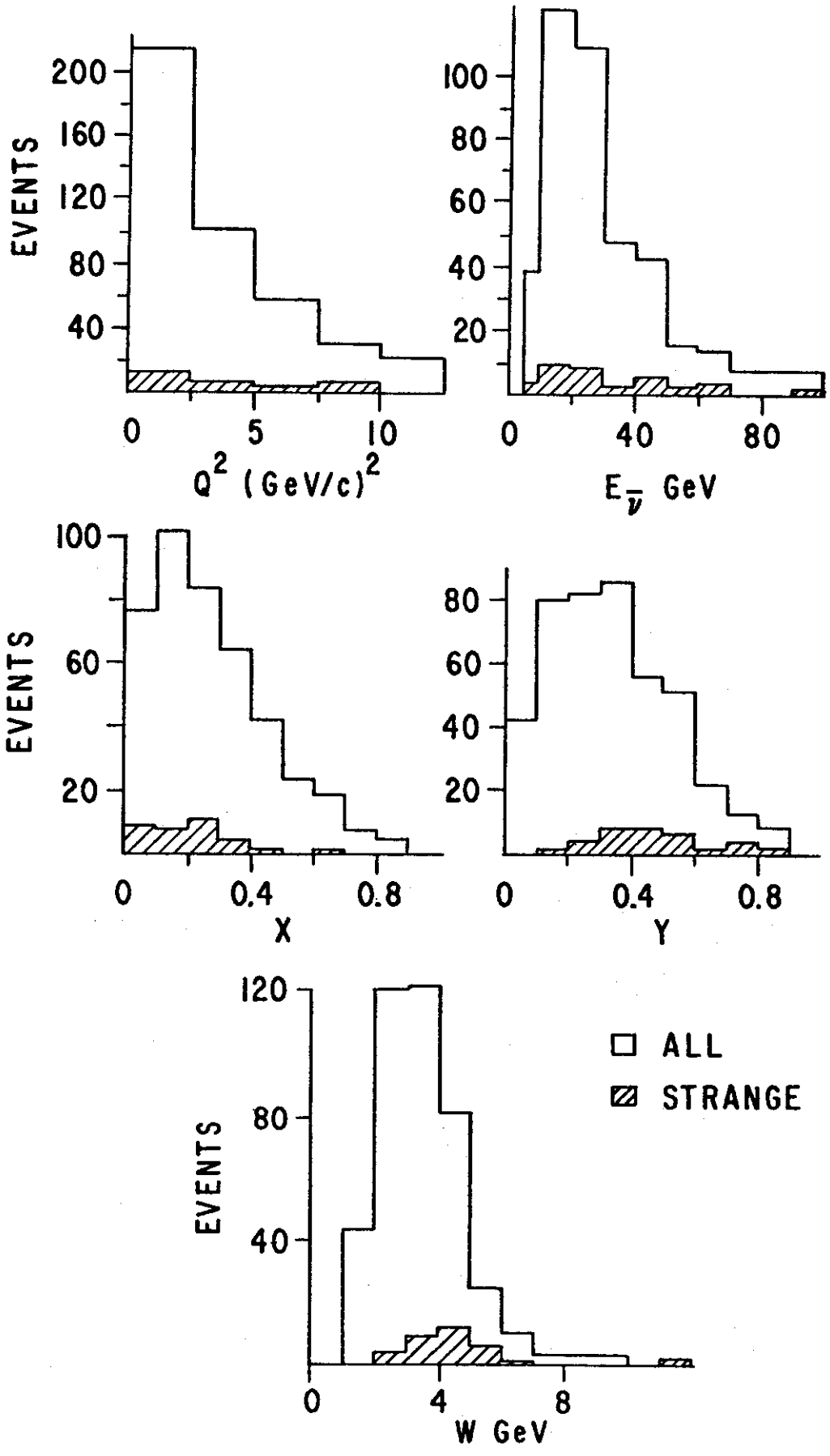
EVENTS
200
160
120
80
40
0
5
10
Q^2 (GeV/c)^2
100
80
60
40
20
0
40
80
$E_{\bar{\nu}}$ GeV
EVENTS
100
60
20
0
0.4
0.8
X
80
60
40
20
0
0.4
0.8
Y
EVENTS
120
80
40
0
4
8
W GeV
ALL
STRANGE

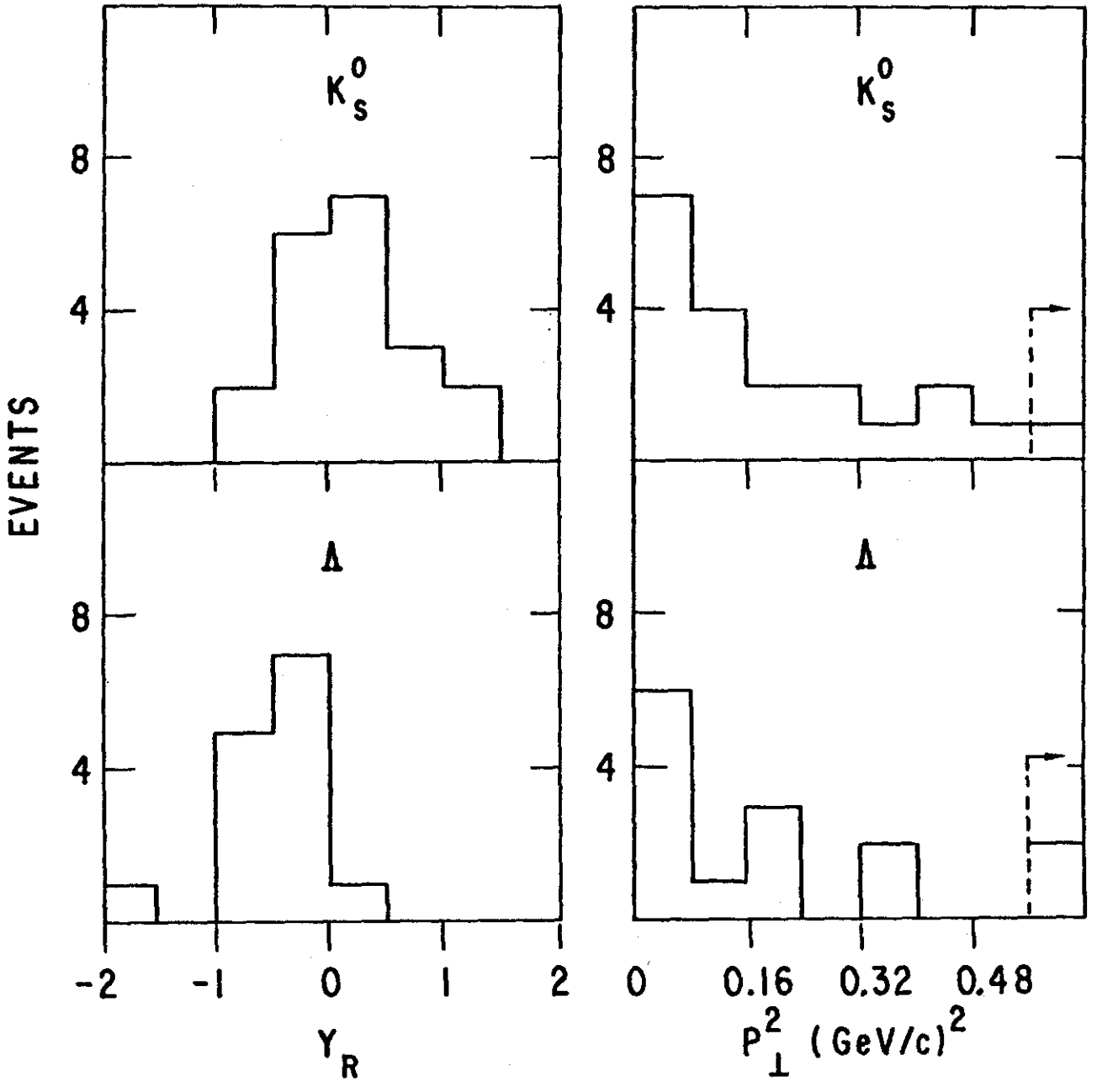
K^0_S
K^0_S
Λ
Λ
EVENTS
8
4
8
4
-2
-1
0
1
2
Y_R
0
0.16
0.32
0.48
$P^2_\perp$ (GeV/c)^2

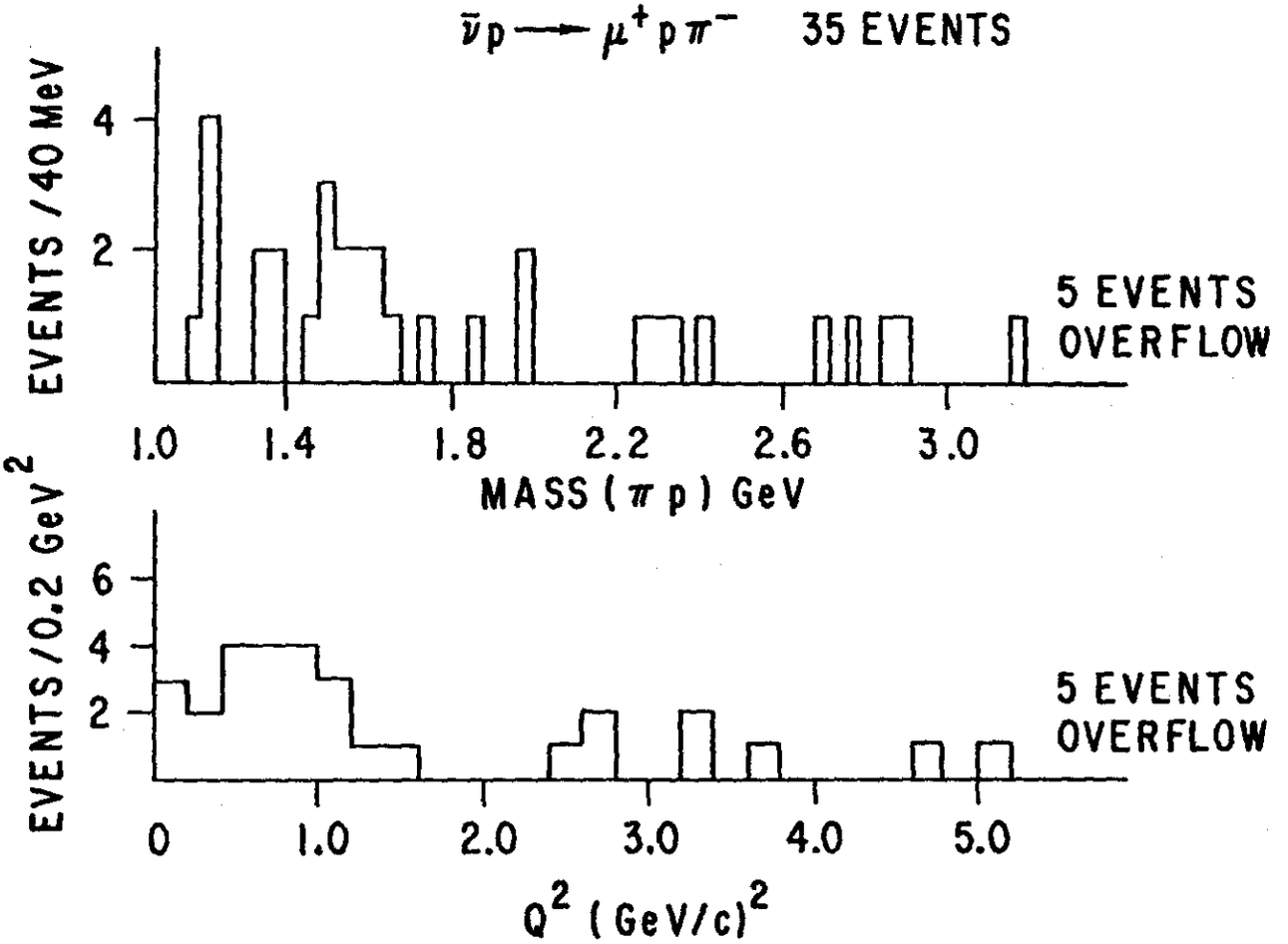
$\bar{\nu}p \longrightarrow \mu^+ p \pi^-$ 35 EVENTS
EVENTS /40 MeV
4
2
5 EVENTS
OVERFLOW
1.0
1.4
1.8
2.2
2.6
3.0
MASS (π p) GeV
EVENTS /0.2 GeV^2
6
4
2
5 EVENTS
OVERFLOW
0
1.0
2.0
3.0
4.0
5.0
Q^2 (GeV/c)^2